Since January 2020 Elsevier has created a COVID-19 resource centre with free information in English and Mandarin on the novel coronavirus COVID-19. The COVID-19 resource centre is hosted on Elsevier Connect, the company's public news and information website.

European Journal of Medicinal Chemistry 68 (2013) 372–384

Contents lists available at ScienceDirect

European Journal of Medicinal Chemistry

journal homepage: http://www.elsevier.com/locate/ejmech

Original article

Development of potent dipeptide-type SARS-CoV 3CL protease inhibitors with novel P3 scaffolds: Design, synthesis, biological evaluation, and docking studies

Pillaiyar Thanigaimalai [a], Sho Konno [a], Takehito Yamamoto [a], Yuji Koiwai [a], Akihiro Taguchi [a], Kentaro Takayama [a], Fumika Yakushiji [a], Kenichi Akaji [b], Shen-En Chen [c], Aurash Naser-Tavakolian [c], Arne Schön [c], Ernesto Freire [c], Yoshio Hayashi [a,*]

[a] Department of Medicinal Chemistry, Tokyo University of Pharmacy and Life Sciences, Tokyo 192-0392, Japan
[b] Department of Medicinal Chemistry, Kyoto Pharmaceutical University, Kyoto 607-8412, Japan
[c] Department of Biology, Johns Hopkins University, Baltimore, MD, USA

ARTICLE INFO

Article history:
Received 19 April 2013
Received in revised form
17 July 2013
Accepted 20 July 2013
Available online 9 August 2013

Keywords:
SARS
SARS-CoV 3CL^{pro}
Dipeptide
Peptidomimetics
Cysteine protease inhibitors

ABSTRACT

We report the design and synthesis of a series of dipeptide-type inhibitors with novel P3 scaffolds that display potent inhibitory activity against SARS-CoV 3CL^{pro}. A docking study involving binding between the dipeptidic lead compound **4** and 3CL^{pro} suggested the modification of a structurally flexible P3 *N*-(3-methoxyphenyl)glycine with various rigid P3 moieties in **4**. The modifications led to the identification of several potent derivatives, including **5c**–**k** and **5n** with the inhibitory activities (K_i or IC_{50}) in the submicromolar to nanomolar range. Compound **5h**, in particular, displayed the most potent inhibitory activity, with a K_i value of 0.006 μM. This potency was 65-fold higher than the potency of the lead compound **4** ($K_i = 0.39$ μM). In addition, the K_i value of **5h** was in very good agreement with the binding affinity (16 nM) observed in isothermal titration calorimetry (ITC). A SAR study around the P3 group in the lead **4** led to the identification of a rigid indole-2-carbonyl unit as one of the best P3 moieties (**5c**). Further optimization showed that a methoxy substitution at the 4-position on the indole unit was highly favorable for enhancing the inhibitory potency.

1. Introduction

Severe acute respiratory syndrome is a highly contagious and fatal respiratory disease that has infected more than 8000 individuals, 10% of which died within a few months of the emergence of the disease between November 2002 and early 2003 [1]. Extensive collaborative research cooperation between the leading experts and the World Health Organization (WHO) led to the rapid identification of a novel coronavirus (CoV) as the etiological agent underlying the pandemic SARS infection. The SARS outbreak was consequently successfully controlled during the beginning of 2003 [2,3]. A reemergence of a SARS-CoV pandemic is still considered to be a potential risk, and new strains of SARS could potentially be more severe than the strains that contributed to the 2003 outbreak. Since 2003, two additional human coronavirus, NL63 and HKU1, have been identified in patients around the world. These new viruses have been characterized and were found to be significantly less lethal than SARS-CoV [4–6]. A new SARS-like virus, HCoV-EMC, was recently identified in at least two individuals, one of whom died [7]. The first case of a fatal respiratory illness similar to the deadly SARS was very recently confirmed in Britain [8]. The possibility of a future SARS-like pandemic remains, and no vaccines or antiviral agents have yet been developed to prevent or treat SARS-like infections.

SARS-CoV encodes a chymotrypsin-like protease (CL^{pro}) that plays a pivotal role in the replication of the virus [9]. Unlike common serine proteases that contain a Ser-His-Asp catalytic triad in the active site, SARS-CoV 3CL^{pro} contains a Cys–His catalytic dyad (Cys145 and His41) that is functionally analogous to the porcine transmissible gastroenteritis virus main protease (Cys145 and His41) and the human coronavirus 229E main protease (Cys145 and His41) [10]. Cys act as a nucleophile, whereas His functions as a general base [10,11]. Since SARS-CoV 3CL^{pro} plays an important role in the virus life cycle, it has been recognized as a viable target for anti-SARS drug development.

Our ongoing efforts have led to the development of several inhibitors with moderate to remarkable potency against SARS-CoV

* Corresponding author. Tel./fax: +81 42 676 3275.
E-mail address: yhayashi@toyaku.ac.jp (Y. Hayashi).

0223-5234/$ – see front matter © 2013 Elsevier Masson SAS. All rights reserved.
http://dx.doi.org/10.1016/j.ejmech.2013.07.037

3CL^{pro}. As shown in Fig. 1, a first tripeptidic lead compound (**1**) bearing an electrophilic ketone as a warhead moiety was developed from the natural peptide sequence after extensive structural modifications [12]. Regarding the mechanism of action, the electrophilic ketone of **1** can be reacted to the active site Cys-SH group resulting in the formation of hemithioketal intermediate between the enzyme and inhibitors to interfere the enzyme function, and hence it was predicted be a reversible inhibitor of SARS-CoV 3CL^{pro}. A subsequent SAR study afforded promising inhibitors **2** and **3** with excellent inhibitory activities (K_i) of 4.1 and 3.1 nM, respectively [13]. Recently, we reported a series of low molecular weight dipeptide-type inhibitors in which the P3 valine moiety was removed form the lead compound **2** (see Fig. 1). This study led to the identification of a compound **4** as a promising lead with an inhibitory activity (K_i) of 0.39 μM (Fig. 2) [14]. From a structural point of view, the P3 *N*-arylglycyl moiety was recognized as crucial to the activity of **4**, as the amine functionality of glycyl moiety formed a hydrogen bond with the backbone amino acid residue Glu166 of 3CL^{pro} in the docking study.

This study was extended, as reported here, by rigidifying the P3 *N*-arylglycyl unit in **4** in search of a more suitable motif with a favorable conformation would provide better interactions and increase the inhibitory activity toward SARS-CoV 3CL^{pro}. Accordingly, we designed and synthesized a series of dipeptide-type inhibitors with novel P3 scaffolds and tested the inhibitory activities of these compounds against SARS-CoV 3CL^{pro}. Several analogs were identified as exhibiting potent inhibitory activities relative to the lead compound **4**. In particular, a compound bearing a P3 4-methoxyindole-2-carbonyl group (**5h**) exhibited excellent inhibitory activity, with a K_i or IC_{50} value of 0.006 or 0.74 μM, respectively. Extensive molecular docking studies of some compounds were conducted to model the binding interactions of these inhibitors.

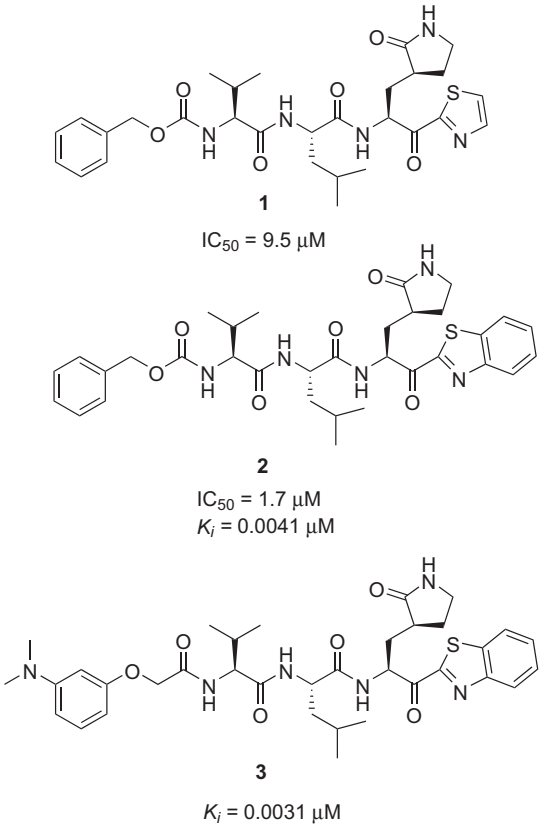

Fig. 1. Structures of potent tripeptidomimetics (**1**–**3**).

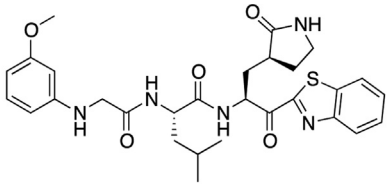

4

K_i = 0.39 μM

IC_{50} = 10.0 μM

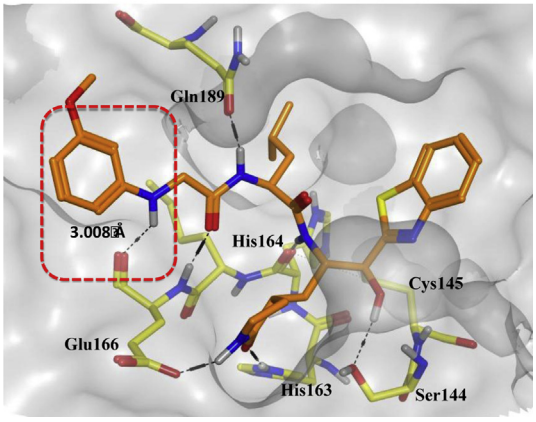

Fig. 2. Docking pose of the lead compound **4** with the SARS-CoV 3CL protease active site. Only residues that are contacted with the ligand (**4**) are highlighted.

2. Results and discussion

2.1. Chemistry

The synthesis of the target compounds **5a**–**r** was envisioned as the assembly of two key fragments: the peptidics **14** and the C-terminal benzothiazole derivative **18** (Schemes 1 and 2). As shown in Scheme 1, the peptidic intermediates **14a**–**r** were synthesized *via* a coupling reaction between various carboxylic acids (**8a**–**r**) and leucine *tert*-butyl ester (**12**), followed by deprotection of *tert*-butyl group. The carboxylic acids, such as 5-oxopyrrolidine-2-carboxylic acid (**8a**), 1*H*-pyrrole-2-carboxylic acid (**8b**), 1*H*-indole-2-carboxylic acid (**8c**), 5-methoxy-1*H*-indole-2-carboxylic acid (**8d**), 5-hydroxy-1*H*-indole-2-carboxylic acid (**8e**), 5-chloro-1*H*-indole-

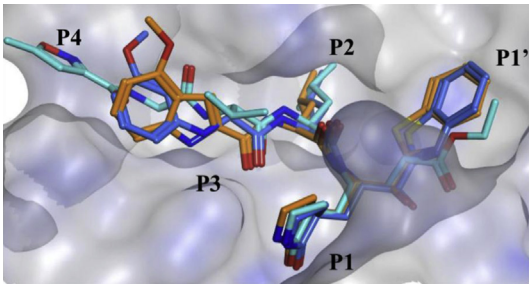

Fig. 3. Molecular dynamics simulated pose of the compound **5h** (orange stick) bound to SARS-CoV 3CL^{pro} (PDB ID: 1WOF). (A) Overlapped view of **5h** with an original vinyl ester (light blue stick) and the lead compound **4** (blue stick). The **5h** moieties P1′–P2 interacted with the same region of the protease as the lead compound **4** and original ligand. The heterocycle unit mimics the P3-valine of the reported ligand and the phenyl ring in indole unit partially occupying the S4-pocket, respectively. The rigid P3-4-methoxyindole unit in **5h** occupying with an appropriate volume and favorable conformation compared to the structurally flexible *N*-(3-methoxyphenyl)glycyl in **4**. (For interpretation of the references to color in this figure legend, the reader is referred to the web version of this article.)

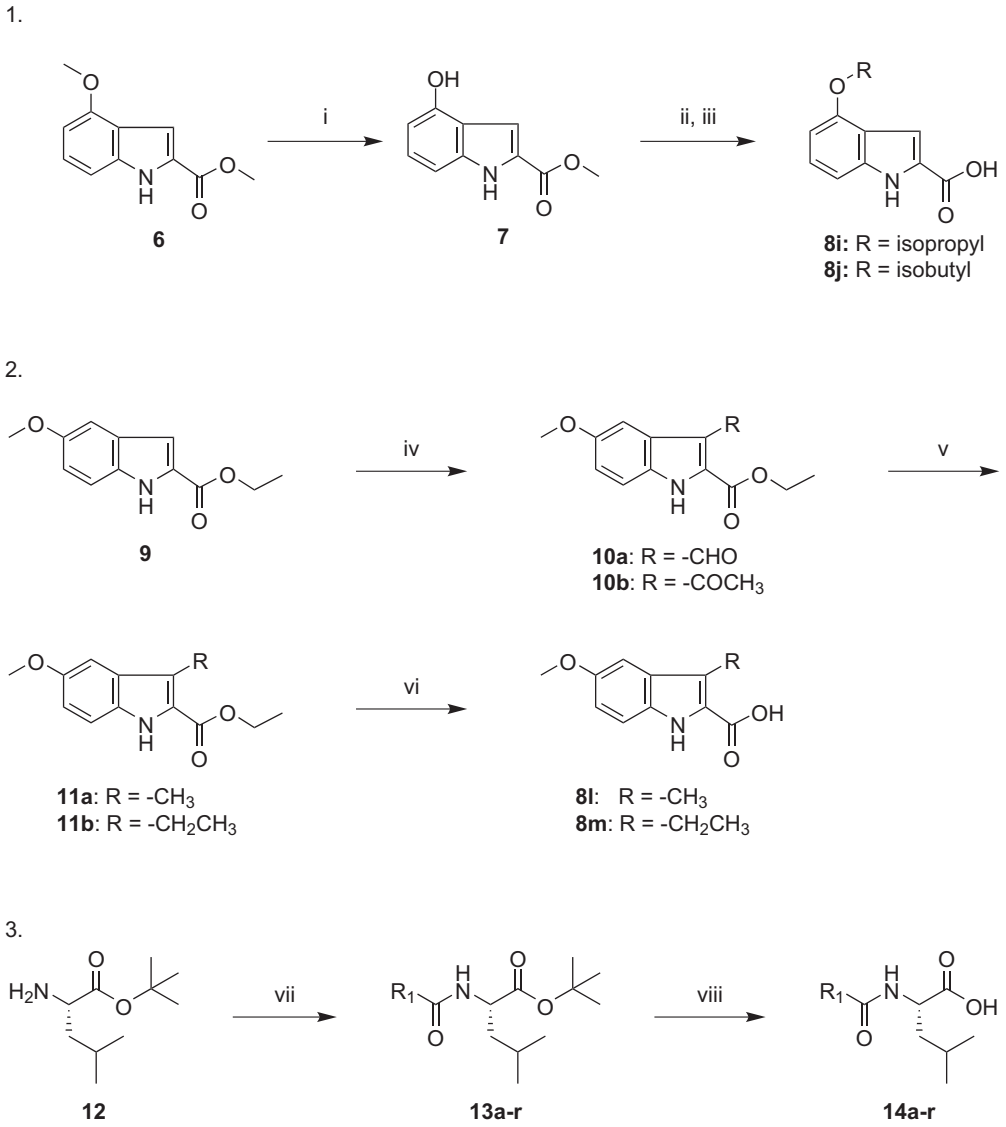

Scheme 1. Synthetic outline for the preparation of **8l**, **8m**, **8i**, **8j** and **14** Reagents and conditions: i) BBr_3 (1 M in DCM), rt, 2 h; ii) DEAD, PPh_3, *i*-PrOH or *i*-BuOH, THF, rt, 30 min; iii) $LiOH \cdot H_2O$, THF, 50 °C, 12 h; iv) $POCl_3$/DMF, 100 °C, 2 h or CH_3COCl, anhydrous $AlCl_3$, 1,2-dichloroethane, reflux, 2 h; v) Et_3SiH, CF_3COOH, rt, 2 h; vi) 4 M NaOH, ethanol, 60 °C, 2 h; vii) **8**, EDC·HCl, $HOBt \cdot H_2O$, TEA, DMF, 0 °C-rt, 2 h; viii) TFA, CH_2Cl_2, 0 °C-rt, 1 h, and subsequent coupling reaction without further characterizations. Note: the substituents R and R_1 were indicated in Table 1.

2-carboxylic acid (**8f**), 6-methoxy-1*H*-indole-2-carboxylic acid (**8g**), 4-methoxy-1*H*-indole-2-carboxylic acid (**8h**), 4-hydroxy-1*H*-indole-2-carboxylic acid (**8k**), 1*H*-benzo[*d*]imidazole-2-carboxylic acid (**8n**), benzo[*d*]thiazole-2-carboxylic acid (**8o**), indoline-2-carboxylic acid (**8p**), benzofuran-2-carboxylic acid (**8q**), and 1*H*-indole-3-carboxylic acid (**8r**) were commercially available.

The carboxylic acids **8i**, **8j**, **8l**, and **8m** were synthesized as shown in Scheme 1. Briefly, the commercially available methyl indole-2-carboxylate **6** underwent *O*-demethylation in the presence of boron tribromide (BBr_3) to produce the corresponding 4-hydroxyindole ester **7** [15,16], which was subsequently treated with various alcohols under Mitsunobu conditions using diethyl azodicarboxylate (DEAD) and triphenylphosphine (PPh_3) in THF, followed by deprotection with lithium hydroxide·water ($LiOH \cdot H_2O$) to furnish the 4-isopropoxy (**8i**) and/or 4-isobutyloxy indole-2-carboxylic acid (**8j**), respectively [15,17].

The commercially available 5-methoxyindole-2-caboxylic acid ethyl ester **9** was submitted to a Vilsmeier–Haack formylation in the presence of phosphoryloxy chloride ($POCl_3$) in DMF to produce **10a** [18,19]. On the other hand, acylation of **9** with acetyl chloride in the presence of anhydrous aluminum chloride ($AlCl_3$) afforded compound **10b** [19,20]. Both the indole-3-formaldehyde (**10a**) and the indole-3-acetyl (**10b**) derivatives were reduced in the presence of triethyl silylhydride (Et_3SiH) [19] to furnish **11a** and **11b**, which were hydrolyzed to afford the corresponding indole-2-carboxylic acids **8l** and **8m**, respectively.

The synthesis of the peptidic fragments **13a**–**r** was achieved from the leucine *tert*-butyl ester (**12**) in the presence of various carboxylic acids (**8**) *via* a 1-ethyl-3-(3-dimethylaminopropyl)carbodiimide (EDC) –1-hydroxybenzotriazole (HOBt)-mediated coupling method in the presence of triethylamine (TEA) in DMF. The N-protected amino acid *tert*-butyl esters (**13**) were subsequently deprotected with trifluoroacetic acid/water (10:1) over 1 h to afford the N-protected amino acids (**14a**–**r**), which were used directly in subsequent steps.

The synthesis of the other key intermediate **18** was achieved using a method reported previously [12–14]. Briefly, the optically pure L-glutamic acid ester **15** was converted to the γ-lactam-acid

16 [21,22] by treatment with bromoacetonitrile, followed by reduction with PtO_2 (5%), cyclization, and hydrolysis (Scheme 2). Further coupling of **16** to *N*,*O*-dimethylhydroxylamine *via* the EDC–HOBt method afforded the Weinreb amide **17** [21]. The Weinreb amide **17** was then coupled to benzothiazole in the presence of *n*-butyl lithium (*n*-BuLi) at −78 °C to furnish **18**, which was then deprotected and subsequently coupled to the peptides **14** in the presence of *O*-benzotriazole- *N*,*N*,*N*′,*N*′-tetramethyluroniumhexafluoro phosphate (HBTU) and DIPEA in DMF to afford the title compounds **5a**–**r**. All compounds were purified by reverse phase HPLC for the biological evaluation and characterized by ^{1}H NMR, ^{13}C NMR, and mass spectrometry. The purity of each compound exceeded 95%.

2.2. Biological assay

The K_i or IC_{50} values of the synthesized compounds against SARS-CoV $3CL^{pro}$ are listed in Tables 1 and 2. The compounds were subjected to a fluorometric protease inhibitory assay using a procedure similar to that mentioned in earlier studies [22,23]. Briefly, the kinetic parameters were determined at a constant substrate concentration, and the inhibitor concentrations were varied to assess the K_i values [12–14]. The IC_{50} values were determined only for certain potent inhibitors, based on the apparent decrease in the substrate concentration (H-TSAVLQSGFRK-NH_2) upon digestion by R188I SARS-CoV $3CL^{pro}$, as described previously [24–26]. The cleavage reaction was monitored by analytical HPLC, and the cleavage rates were calculated from the decrease in the substrate peak area. Tables 1 and 2 report the K_i or IC_{50} values as the mean of 3 independent experiments.

2.3. Structure–activity relationship study

In a previous study, we reported a series of low molecular weight dipeptide-type SARS-CoV $3CL^{pro}$ inhibitors. Among them, compound **4** bearing P3 *N*-(3-methoxyphenyl)glycyl exhibited potent inhibitory activity with a K_i value of 0.39 μM. In this study, we envisioned that substitutions at the P3 *N*-arylglycyl unit in **4** could improve the inhibitory potency against $3CL^{pro}$. Therefore, we designed and synthesized a series of analogs bearing a rigid P3 motif for evaluation against SARS-CoV $3CL^{pro}$. In a first attempt as shown in Table 1, the *N*-(3-methoxyphenyl)glycyl unit was replaced with the DL-pyroglutamyl (**5a**; K_i = 2.70 μM) or the pyrrole-2-carbonyl (**5b**; K_i = 1.70 μM) as a rigid P3 scaffold in **4**. The inhibitory activities of the resulting compounds were dramatically reduced compared to the activity of **4** (K_i = 0.39 μM). On the other hand, the introduction of an indole-2-carbonyl unit (**5c**; K_i = 0.065 μM or IC_{50} = 1.50 μM) yielded a 40- or 25-fold higher inhibitory potency relative to **5a** or **5b**, respectively, and a 6-fold more potent activity relative to **4**. These studies suggested that the rigid indole-2-carbonyl, which was introduced in place of the P3 moiety (*N*-(3-methoxyphenyl)glycyl) in the lead compound **4**, displayed appreciable inhibitory activity. Thus, compound **5c** served as a lead compound for further optimization steps.

The substituent effects at different positions on the P3 indole unit in **5c** were investigated by introducing a wide variety of substituents. Initially, substituents were introduced at the 5-position of the indole unit in **5c**, including 5-methoxy (**5d**; K_i = 0.067 μM or IC_{50} = 4.60 μM), 5-hydroxyl (**5e**; K_i = 0.160 μM), or 5-chloro (**5f**; K_i = 0.028 μM or IC_{50} = 4.80 μM). This result suggested that the 5-chloro substituent on the indole unit (**5f**) exhibited good inhibitory potency relative to, respectively, lead compound **5c**, 5-methoxy (**5d**) and 5-hydroxy (**5e**) derivatives. Next, a methoxy group was introduced at the 6-position on the indole unit, as shown in **5g** (K_i = 0.333 μM). The activity of **5g** was lower than the activity of **5d**; thus, the substitution at the 6-position on the P3 indole-2-carbonyl in **5c** did not significantly improve the inhibitory activity. On the other hand, the methoxy substitution at the 4-position on the indole unit (**5h**; K_i = 0.006 μM or IC_{50} = 0.74 μM) exhibited excellent inhibitory activity, with 10- or 55-fold increases in activity relative to, respectively, the 5-methoxy (**5d**) or 6-methoxy (**5g**) derivatives. This finding revealed that the methoxy substitution at the 4-position on the indole unit in **5c** significantly improved the inhibitory activity.

The 4-methoxy group on the indole unit of **5h** was examined by substitution with 4-isopropoxyl (**5i**; K_i = 0.048 μM), 4-isobutyloxyl (**5j**; K_i = 0.030 μM or IC_{50} = 5.20 μM), or 4-hydroxyl (**5k**; K_i = 0.026 μM or IC_{50} = 1.30 μM) moieties; however, the inhibitory activities of **5i**, **5j**, or **5k** were lower than the activity of the 4-methoxy derivative **5h**. This study strongly suggested that the optimal methoxy group at the 4-position on the indole in **5c** was more important than the isopropoxy, isobutyloxy, or hydroxyl groups.

We tested the introduction of substitutions at the 3-position on the indole unit by starting with the lead compound **5d**. The 3-methyl (**5l**; K_i = 6.71 μM) or 3-ethyl (**5m**; K_i = 7.51 μM) groups were introduced first; however, the inhibitory activities of both **5l** and **5m** were severely reduced relative to the activity of **5d**. These

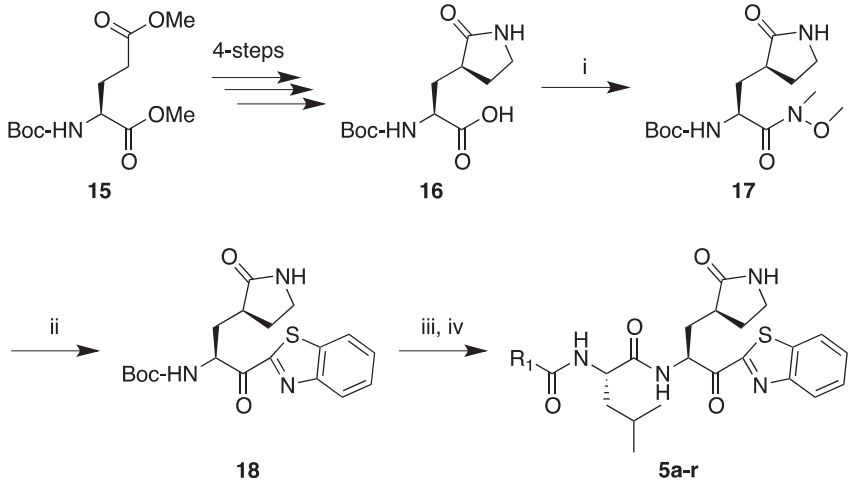

Scheme 2. Synthetic outline for the preparation of **5a**–**r** Reagents and conditions: i) HN(OMe)Me·HCl, EDC·HCl, HOBt·H_2O, Et_3N, DMF, 0 °C-rt, 2 h; ii) benzothiazole, *n*-BuLi, THF, −78 °C-rt, 3–5 h; iii) TFA, CH_2Cl_2, 0 °C-rt, 1 h; iv) **14**, HBTU, DIPEA, DMF, 0 °C-rt, 2 h followed by HPLC purification. Note: the substituents R and R_1 were indicated in Table 1.

Table 1
SARS-CoV 3CL^{pro} inhibitory activities (K_i) of **5a**–**r**.

Entry no.	Inhibitors	K_i (μM)	Entry no.	Inhibitors	K_i (μM)
5a	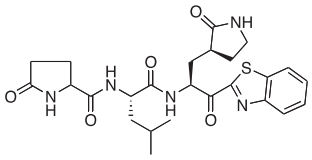	2.7	**5j**	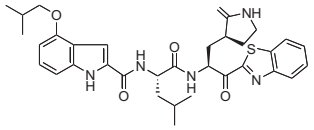	0.030
5b	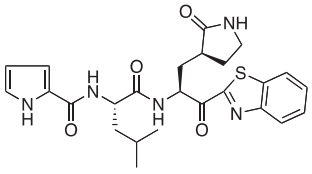	1.7	**5k**	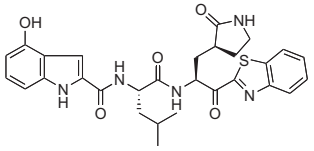	0.026
5c	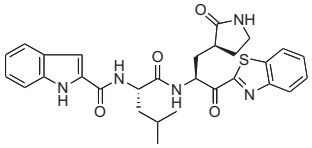	0.065	**5l**	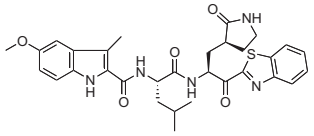	6.7
5d	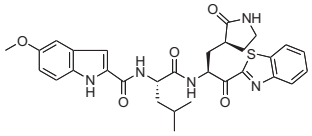	0.067	**5m**	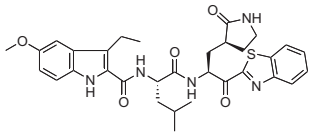	7.5
5e	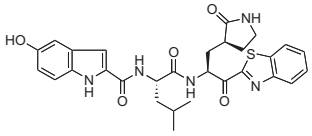	0.16	**5n**	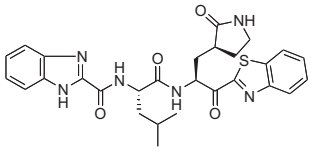	0.022
5f	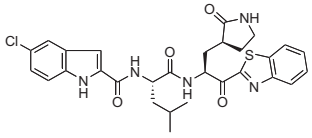	0.028	**5o**	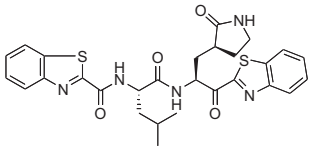	0.80
5g	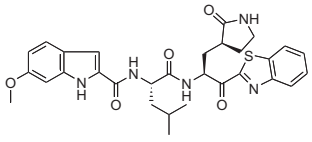	0.33	**5p**	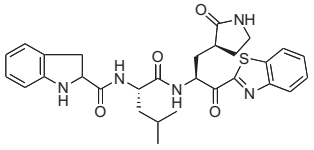	0.12
5h	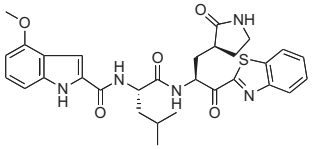	0.0063	**5q**	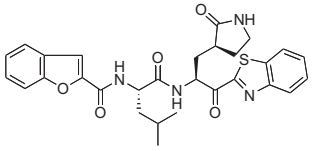	14
5i	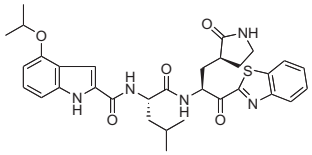	0.048	**5r**	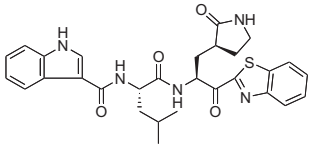	0.68

results suggested that substitutions at the 3-position on the indole unit were not a fruitful direction of study.

The P3 indole unit in **5c** was next examined by varying the heterocycle by replacing it with benzimidazole, benzothiazole, benzofuran, or indoline scaffolds. The compounds bearing a benzimidazole (**5n**; K_i = 0.022, IC_{50} = 1.30 μM) exhibited 3-fold potent inhibitory activity than the lead compound **5c**; however, the other indoline (**5p**; K_i = 0.120 μM) or benzothiazole (**5o**; K_i = 0.800 μM) or a benzofuran (**5q**; K_i = 14.1 μM), were lower than the activity of the lead compound **5c**. Compound **5q**, bearing

Table 2
SARS-CoV $3CL^{pro}$ inhibitory activities (IC_{50}) of selected compounds.

Entry no.	IC_{50} (μM)
5c	1.50
5d	4.60
5f	4.80
5h	0.74
5j	5.20
5k	1.50
5n	1.30

a benzofuran unit, displayed a severely reduced inhibitory potency compared to the lead compound **5c**. The observed low activity of **5q** was attributed to the disruption of hydrogen bonding interactions at the P3 position. This result suggested that the hydrogen bonding properties of the amine moiety of the indole unit were very important for achieving effective inhibitory activities (see Fig. 4).

The position of the carbonyl substitution on the indole unit in **5c** was examined next. The inhibitory activity of the derivative (**5r**; $K_i = 0.683$ μM) bearing an indole-3-carbonyl was reduced relative to the activity of the compound bearing an indole-2-carbonyl (**5c**; $K_i = 0.065$ μM). The substitution may have interrupted a hydrogen bonding interaction with the protease (see Fig. 4). These results strongly suggested that the 2-carbonyl substitution on the indole unit in **5c** was important to the inhibitory potency.

2.4. Molecular docking study

The binding mode of the most potent compound, **5h** was computationally modeled using a three-dimensional structure of SARS-CoV $3CL^{pro}$ based on the reported crystal structure [27]. A procedure similar to the procedure described previously was used

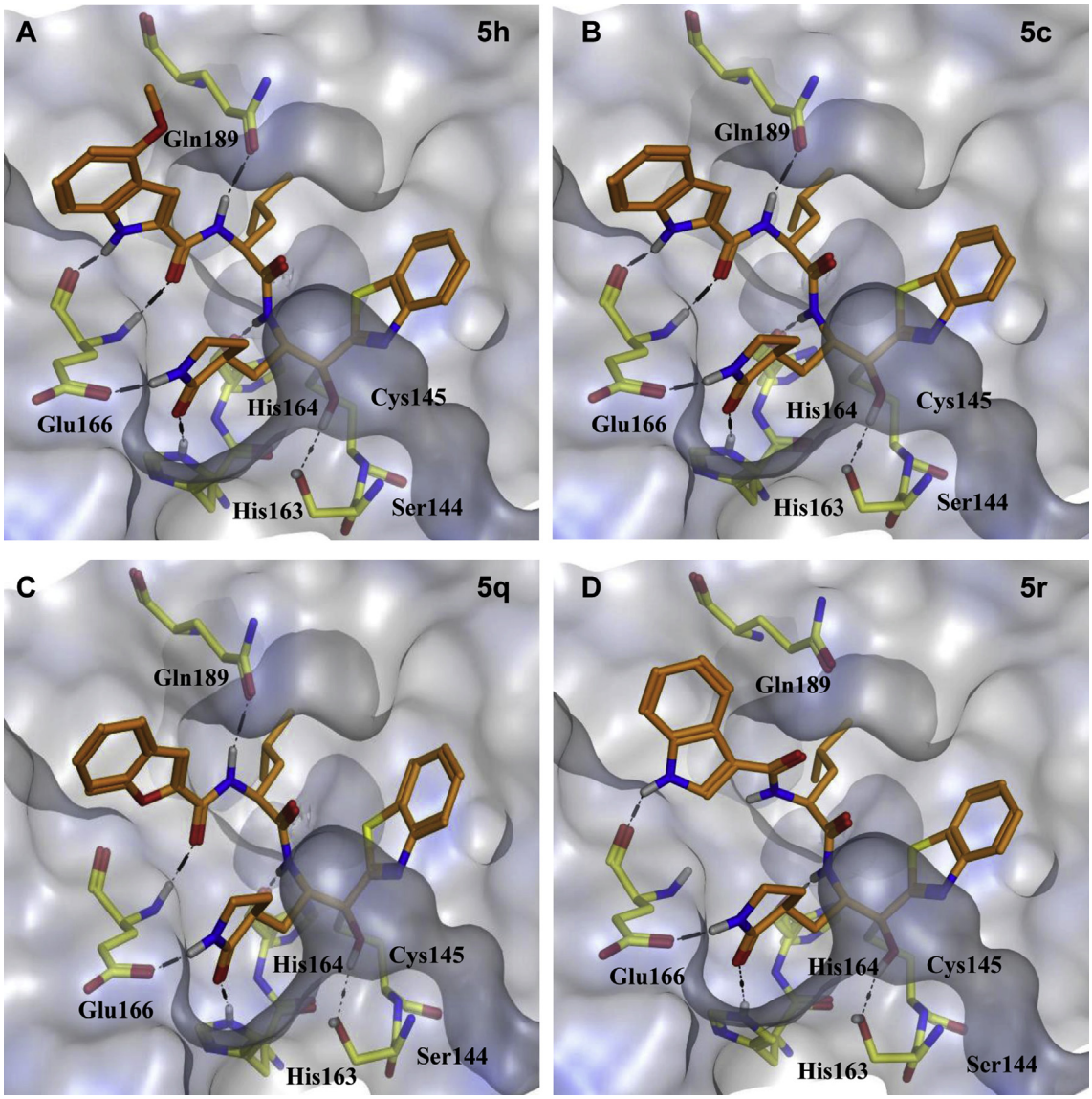

Fig. 4. Molecular docking pose and binding interactions of compounds **5h**, **5c**, **5q** and **5r** (orange sticks) bound to SARS-CoV $3CL^{pro}$ (PDB ID: 1WOF). Only the residues (yellow color), which are engaged in binding to the ligands (orange sticks), are highlighted. Dotted black lines represent the hydrogen bonding interaction. (A) Mode of interactions of **5h**, particularly the P3-indole-2-carbonyl to the Glu166 and Gln189 of $3CL^{pro}$, which was also observed for compound **5c** (B); (C) The hydrogen bond between Glu-166 and P3-benzofuran moiety was omitted in the case of **5q**; (D) The indole-3-carbonyl of **5r** looses their hydrogen bonding interactions to Glu166 and Gln189. (For interpretation of the references to color in this figure legend, the reader is referred to the web version of this article.)

here [12–14]. The molecular docking of **5h** (orange sticks) was examined, in comparison with a lead compound **4** (blue sticks) and a structurally similar tripeptidic ligand (light blue sticks), the docking structure of which was elucidated by X-ray crystallography (PDB ID. 1WOF, K_i = 10.7 μM, Fig. 3) [27]. Several minimization processes were performed using the MMFF94X force field to model the solvation environment surrounding the inhibitor. A molecular simulation was subsequently performed. As shown in Fig. 3, the **5h** moieties P1′–P2 interacted with the same region of the protease as did the lead compound **4** and the original ligand. The heterocycle unit mimicked the P3 valine of the reported substrate, and the phenyl ring in the indole unit partially occupied the S4-pocket. The rigid P3 moiety (4-methoxyindole unit) of **5h** appeared to occupy a region of the active site with an appropriate volume and in a conformation that was more favorable than the conformation of the structurally flexible *N*-(3-methoxyphenyl)glycyl moiety in **4**. Indeed, the fit of the rigid P3 moiety of **5h** may have contributed to the 65-fold higher inhibitory potency of **5h** as compared to **4**. The detailed interactions between **5h** and the active site are shown in Fig. 4A. Hydrogen bonds between the amine moiety (-NH) of the indole unit and the backbone amino acid residue Glu166 of 3CL^{pro} were observed with a bond length of 2.673 Å.

Insight into the structure–activity relationships was sought by performing docking studies and analyzing the binding interactions of certain compounds that displayed notable variations in their inhibitory activities (Fig. 4B–D). The initial lead compound **5c**, bearing a P3 indole-2-carbonyl unit, was docked (Fig. 4B), revealing hydrogen bonding interactions similar to those predicted for **5h** (Fig. 4A); however, **5q**, bearing a benzofuran-2-carbonyl P3 moiety, could not form a hydrogen bond interaction with the backbone amino acid residue Glu166 (Fig. 4C). The loss of hydrogen bond interactions could have reduced the inhibitory activity of compound **5q** (K_i = 14.1 μM) compared to the activity of compound **5c** (K_i = 0.065 μM). The compound **5r** (K_i = 0.683 μM), bearing an indole-3-carbonyl unit, engaged in two fewer hydrogen bonding interactions to the amino acid residues Glu166 and Gln189 of the protease relative to **5c**, as shown in Fig. 4D. This study revealed that the optimal positioning of a carbonyl unit on the indole unit was very important for achieving a potent inhibitory activity.

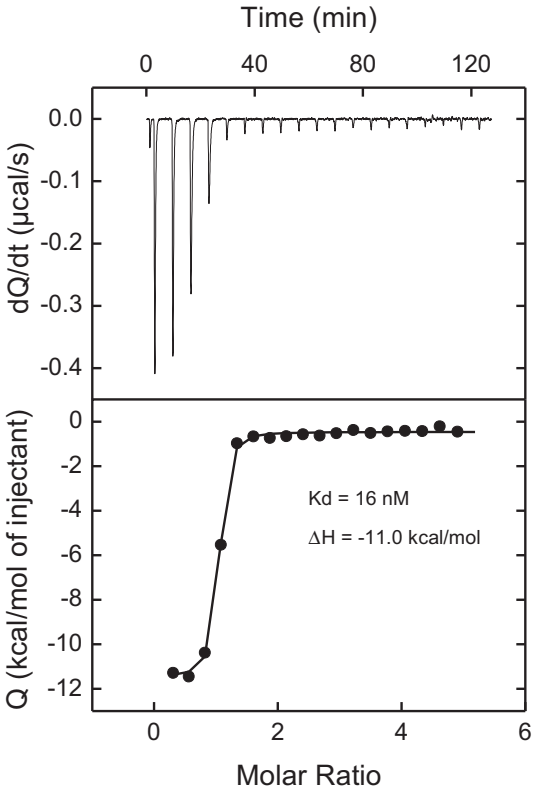

Fig. 5. Isothermal titration calorimetry of compound **5h**.

2.5. Isothermal titration calorimetry study

In order to evaluate in-depth bending interaction between the most potent compound **5h** and the SARS protease, the isothermal titration calorimetry study was demonstrated (Fig. 5). The titration was performed at 25 °C by injecting 10 μL aliquots of protease solution into the calorimetric cell (volume ~ 1.4 mL) containing the inhibitor **5h** at a concentration of 6 μM. The concentration of protease in the syringe was 109 μM. The heat evolved upon each injection of protease was obtained from the integral of the calorimetric signal. The heat associated with inhibitor binding was obtained by subtracting the heat of dilution from the heat of reaction. The individual heats were plotted against the molar ratio, and the enthalpy change (ΔH) and association constant ($K_a = 1/K_d$) were obtained by nonlinear regression of the data. The binding affinity of compound **5h** was 16 nM which is in very good agreement with the K_i value (0.006 μM).

3. Conclusion

We describe here the design, synthesis, and biological evaluation of a series of dipeptide-type inhibitors with novel P3 scaffolds against SARS-CoV 3CL^{pro}. A docking study involving binding between the dipeptidic lead compound **4** and 3CL^{pro} motivated the modification of a flexible P3 *N*-(3-methoxyphenyl)glycine in **4** to various structurally rigid moieties. This modification led to the identification of several potent derivatives, including **5c**–**k** and **5n**, which displayed inhibitory activities (K_i or IC_{50}) in the submicromolar to nanomolar range. Compounds **5c**, **5f**, **5h**, **5k** and **5n**, in particular, exhibited the most potent inhibitory activities, with K_i values of 0.065, 0.028, 0.006 0.026 and 0.022 μM, respectively. These compounds are attractive leads for a further development effort toward potent peptidomimetics with suitable pharmaceutical profiles. A SAR study around the P3 site in the lead compound **4** led to the identification of a rigid indole-2-carbonyl unit as one of the best P3 moieties (**5c**). Further optimization of **5c** showed that an optimal methoxy substitution at the 4-position on the P3 indole unit enhanced the inhibitory activity significantly. The 2-carbonyl substitution on the P3 indole was also found to be important to the inhibitory potency against SARS-CoV 3CL^{pro}.

4. Experimental section

4.1. Materials and methods

Reagents and solvents were purchased from Wako Pure Chemical Ind., Ltd. (Osaka, Japan) and Aldrich Chemical Co. Inc. (Milwaukee, WI) and were used without further purification. Analytical thin layer chromatography (TLC) was performed on Merck Silica Gel 60F254 pre-coated plates. Preparative HPLC was performed using a C18 reverse-phase column (19 × 100 mm; SunFire Prep C18 OBD™, 5 μm) with a binary solvent system: a linear gradient of CH_3CN in 0.1% aqueous TFA at a flow rate of 6 mL/min. Compounds were detected at 254 nm and 230 nm. All solvents used for HPLC were HPLC-grade. All other chemicals were of analytical grade or better. ^1H and ^{13}C NMR spectra were obtained using a JEOL 400 MHz spectrometer, a Varian Mercury 300 spectrometer (300 MHz), or a BRUKER AV600 spectrometer (600 MHz)

with tetramethylsilane as an internal standard. Chemical shifts (δ) are expressed in ppm using solvent as an internal standard. The multiplicities of the resonance peaks are indicated as singlet (s), broad singlet (bs), doublet (d), triplet (t), quartet (q), and multiplet (m). The *J* values are given in Hz, and the relative number of protons was determined by integration. The solvent used for each spectrum is reported. High-resolution mass spectra (ESI or EI) were recorded on a micromass Q-Tof Ultima API or a JEOL JMS-GCmate BU-20 spectrometer. Mass spectra (ESI) were recorded on LCMS-2010EV (SHIMADZU).

4.2. Synthesis of methyl 4-hydroxy-1H -indole-2-carboxylate (**7**) [17]

To an ice-cold solution of methyl 4-methoxy-1H-indole-2-carboxylate **6** (0.850 g, 4.1 mmol) in DCM (10 mL) was added BBr_3 (1.0 mL in DCM, 4.0 mmol). The solution was stirred for 1 h, and another equivalent (1.0 mL in DCM) of BBr_3 was added. After stirring for another hour, the mixture was poured over crushed ice and the pH was adjusted to 7 by adding solid $NaHCO_3$. The solution was extracted with DCM (60 mL), dried over Na_2SO_4, filtered, and evaporated under reduced pressure to give **7** [17].

4.3. Synthesis of ***8a–r***

The carboxylic acids **8a–h**, **8k** and **8n–r** were commercially available.

4.3.1. Synthesis of 4-isopropoxy-1H-indole-2-carboxylic acid (***8i***) [16]

DEAD (0.227 mL, 2.9 mmol) was slowly added to a solution of 4-hydroxy-1*H*-indole-2-carboxylic acid methyl ester (**7**) (0.800 g, 4.0 mmol), triphenylphosphine (0.750 g, 2.9 mmol), and isopropanol (0.215 mL, 2.90 mmol) in 2 mL THF. Stirring was continued for 30 min, and the solvent was then evaporated. The crude mixture was purified by chromatography to give a pure methyl 4-isopropoxy-1*H*-indole-2-carboxylate, which was dissolved in 5 mL THF. A solution containing $LiOH\cdot H_2O$ (2.94 mmol) in THF:H_2O (10:1) was added, and the mixture was stirred overnight at 50 °C. The solvent was then evaporated, and the residue was partitioned between water and EtOAc. The water layer was acidified with 2 NHCl and extracted twice with EtOAc (50 mL × 2). The combined organic layers were washed with brine, dried over Na_2SO_4, filtered, and evaporated to give **8i** [16].

4.3.2. Synthesis of 4-isobutoxy-1H-indole-2-carboxylic acid (***8j***) [16]

Compound **8j** was synthesized from **7** with isobutanol using methods similar to the method described for the preparation of **8i** [16].

4.3.3. Synthesis of ethyl 3-formyl-5-methoxy-1H-indole-2-carboxylate (***10a***) [19]

A solution of ethyl 5-methoxy-1*H*-indole-2-carboxylate (**9**) (1.68 g, 7.6 mmol) in anhydrous *N*,*N*-dimethylformamide (3 mL) was added dropwise onto an ice-cooled solution of phosphorus oxychloride (1.73 mL, 15 mmol) in DMF (5 mL). The reaction mixture was heated at 110 °C for 2.5 h. After cooling, the reaction was quenched with ice water and made alkaline by the addition of a 2% sodium hydroxide solution. The precipitate was collected and purified by column chromatography to give **10a** [19].

4.3.4. Synthesis of ethyl 3-acetyl-5-methoxy-1H-indole-2-carboxylate (***10b***) [20]

Ethyl 5-methoxy-1*H*-indole-2-carboxylate (**9**) (1.68 g, 7.6 mmol) was added to a mixture of acetyl chloride (0.55 mL, 7.6 mmol) and aluminum chloride (1.07 g, 7.6 mmol) in anhydrous 1,2-dichloroethane (10 mL). The reaction mixture was heated under reflux for 2.5 h. After cooling, the reaction mixture was poured over crushed ice and made acidic by the addition of 3 N HCl. The mixture was extracted with dichloromethane (20 mL × 2). The combined organic layers were washed with brine, dried, and evaporated. The residue was purified by silica gel column chromatography to provide **10b** [20].

4.3.5. Synthesis of ethyl 5-methoxy-3-methyl-1H-indole-2-carboxylate (***11a***)

A mixture of **10a** (1.09 g, 4.40 mmol), triethylsilane (1.43 g, 16.0 mmol), and 2,2,2-trifluoroacetic acid (5.94 mL) was stirred at room temperature for 5 h. After quenching with a saturated solution of sodium carbonate, the mixture was extracted with ethyl acetate (20 mL × 2). The combined organic layers were washed with a saturated solution of sodium bicarbonate, brine, and then the solution was dried. After evaporating the solvent, the residue was purified by column chromatography to give ethyl 5-methoxy-3-methyl-1*H*-indole-2-carboxylate **11a**. Yield 89% from **10a**; yellow solid; ^{1}H NMR (400 MHz, $CDCl_3$): δ 8.57 (br s, 1H), 7.29–7.25 (m, 1H merged with $CDCl_3$), 7.03–6.98 (m, 2H), 4.41 (q, J = 7.2 Hz, 2H), 3.87 (s, 3H), 2.58 (s, 3H), 1.42 (t, J = 7.2 Hz, 3H). HRMS (ESI): *m*/*z* calcd for $C_{13}H_{16}NO_3$ $[M + H]^+$ 234.1130, found 234.1129.

4.3.6. Synthesis of ethyl 3-ethyl-5-methoxy-1H-indole-2-carboxylate (***11b***)

The compound **11b** was synthesized from **10b** using a procedure similar to that described for the preparation of **10a**. Yellow solid; yield 65%; ^{1}H NMR (400 MHz, $CDCl_3$): δ 8.65 (br s, 1H), 7.27–7.20 (m, 1H merged with $CDCl_3$), 7.06–7.04 (m, 1H), 7.00 (dd, J = 8.8, 2.4 Hz, 1H), 4.41 (q, J = 7.2 Hz, 2H), 3.87 (s, 3H), 3.08 (q, J = 7.5 Hz, 2H), 1.42 (t, J = 7.2 Hz, 3H), 1.29–1.23 (t, J = 7.5 Hz, 3H). HRMS (ESI): *m*/*z* calcd for $C_{14}H_{18}NO_3$ $[M + H]^+$ 248.1287, found 248.1285.

4.4. Synthesis of 5-methoxy-3-methyl-1H-indole-2-carboxylic acid (***8l***)

To a solution of the ethyl 5-methoxy-3-methyl-1*H*-indole-2-carboxylate **11a** (0.100 g, 0.35 mmol) in THF (3 mL) at room temperature was added $LiOH\cdot H_2O$ in water (0.102 g, 2.45 mmol). After 3 h stirring, the solvent was completely evaporated under reduced pressure, and the resulting residue was neutralized with 2 N HCl. The solution was extracted with EtOAc (20 mL × 2), dried over Na_2SO_4, filtered, and evaporated under reduced pressure to give the corresponding acids **8l**. Yield 85%; brown solid; ^{1}H NMR (400 MHz, CD_3OD): δ 7.35–7.18 (m, 1H), 7.17–7.00 (m, 1H), 6.92–6.89 (m, 1H), 3.82–3.79 (m, 3H), 2.55 (s, 3H); HRMS (ESI): *m*/*z* calcd for $C_{11}H_{12}NO_3$ $[M + H]^+$ 206.0817, found 206.0818.

4.5. Synthesis of 3-ethyl-5-methoxy-1H-indole-2-carboxylic acid (***8m***)

The synthesis of **8m** was achieved from **11b** using a procedure similar to that described for the preparation of **8l**. Yield 81%; brown solid; ^{1}H NMR (400 MHz, CD_3OD): δ 7.38–7.23 (m, 1H), 7.06 (s, 1H), 6.98 (d, J = 8.9 Hz, 1H), 3.88 (s, 3H), 3.11 (q, J = 7.4 Hz, 2H), 1.28 (t, J = 7.5 Hz, 3H); HRMS (ESI): *m*/*z* calcd for $C_{12}H_{14}NO_3$ $[M + H]^+$ 220.0974, found 220.0975.

4.6. General synthetic procedure for the preparation of ***13a–r***

To a solution of the commercially available L-leucine *tert*-butyl ester (**12**, 0.89 mmol) in DMF (15 mL) were added an appropriate carboxylic acid (**8**, 1.1 mmol), $HOBt\cdot H_2O$ (1.1 mmol), and $EDC\cdot HCl$ (1.1 mmol). The resulting solution was cooled to 0 °C under ice

bath conditions, and TEA was added dropwise. After 5 min, the ice bath was removed, and the mixture was allowed to stir for 2 h at ambient temperature. DMF was removed under high vacuum, and the resulting residue was dissolved in EtOAc (30 mL). The organic layer was washed with 5% citric acid (20 mL × 2), 5% $NaHCO_3$ (20 mL × 2), and brine (20 mL). The solution was dried over Na_2SO_4, filtered, and evaporated under reduced pressure to give compound **13**. The resulting crude compound was purified by silica gel column chromatography using hexane–EtOAc as eluents.

4.6.1. (2S)-tert-Butyl 4-methyl-2-(5-oxopyrrolidine-2-carboxamido)pentanoate (**13a**)

Yield 51% from **12** with 5-oxopyrrolidine-2-carboxylic acid (**8a**); white solid; ^{1}H NMR (400 MHz, $CDCl_3$): δ 4.58–4.44 (m, 1H), 4.21–4.16 (m, 1H), 2.60–2.48 (m, 1H), 2.47–2.38 (m, 1H), 2.37–2.25 (m, 1H), 2.24–2.12 (m, 1H), 1.65–1.51 (m, 3H), 1.45 (s, 9H), 0.95–0.83 (m, 6H); HRMS (ESI): *m*/*z* calcd for $C_{15}H_{27}N_2O_4$ $[M + H]^+$ 299.1971, found 299.1973.

4.6.2. (S)-tert-Butyl 2-(1H-pyrrole-2-carboxamido)-4-methylpentanoate (**13b**)

Yield 63% from **12** with 1*H*-pyrrole-2-carboxylic acid (**8b**); white solid; ^{1}H NMR (400 MHz, $CDCl_3$): δ 6.94–6.89 (m, 1H), 6.65–6.62 (m, 1H), 6.35 (d, J = 8.3 Hz, 1H), 6.24–6.20 (m, 1H), 4.74–4.65 (m, 1H), 1.76–1.53 (m, 3H), 1.48 (s, 9H), 0.97 (t, J = 6.8 Hz, 6H); HRMS (ESI): *m*/*z* calcd for $C_{15}H_{25}N_2O_3$ $[M + H]^+$ 281.1865, found 281.1862.

4.6.3. (S)-tert-Butyl 2-(1H-indole-2-carboxamido)-4-methylpentanoate (**13c**)

Yield 54% from **12** with 1*H*-indole-2-carboxylic acid (**8c**); yellow solid; ^{1}H NMR (400 MHz, $CDCl_3$): δ 9.10 (s, 1H), 7.66 (d, J = 8.0 Hz, 1H), 7.41 (d, J = 8.2 Hz, 1H), 7.30–7.26 (m, 1H merged with $CDCl_3$), 7.14 (t, J = 8.0 Hz, 1H), 6.92 (s, 1H), 6.60 (d, J = 8.4 Hz, 1H), 4.78–4.71 (m, 1H), 1.79–1.58 (m, 3H), 1.50 (s, 9H), 1.00 (t, J = 6.0 Hz, 6H); HRMS (ESI): *m*/*z* calcd for $C_{19}H_{27}N_2O_3$ $[M + H]^+$ 331.2022, found 331.2012.

4.6.4. (S)-tert-Butyl 2-(5-methoxy-1H-indole-2-carboxamido)-4-methylpentanoate (**13d**)

Yield 61% from **12** with 5-methoxy-1*H*-indole-2-carboxylic acid (**8d**); fluorescent solid; ^{1}H NMR (400 MHz, $CDCl_3$): δ 9.33 (s, 1H), 7.49 (d, J = 8.7 Hz, 1H), 6.88–6.84 (m, 2H), 6.80 (dd, J = 8.8, 2.2 Hz, 1H), 6.69 (d, J = 8.4 Hz, 1H), 4.80–4.70 (m, 1H), 3.85 (s, 3H), 1.80–1.61 (m, 3H), 1.50 (s, 9H), 0.99 (t, J = 6.2 Hz, 6H); HRMS (ESI): *m*/*z* calcd for $C_{20}H_{29}N_2O_4$ $[M + H]^+$ 361.2127, found 361.2116.

4.6.5. (S)-tert-Butyl 2-(5-hydroxy-1H-indole-2-carboxamido)-4-methylpentanoate (**13e**)

Yield 63% from **12** with 5-hydroxy-1*H*-indole-2-carboxylic acid (**8e**); yellow solid; ^{1}H NMR (400 MHz, CD_3OD): δ 7.97 (br s, 1H), 7.88 (d, J = 8.4 Hz, 1H), 7.74 (d, J = 8.4 Hz, 1H), 7.27 (d, J = 8.8 Hz, 1H), 7.02 (s, 1H), 6.95 (d, J = 2.2 Hz, 1H), 6.81 (dd, J = 8.9, 2.4 Hz, 1H), 4.60–4.51 (m, 1H), 1.80–1.64 (m, 3H), 1.47 (s, 9H), 1.00 (d, J = 6.2 Hz, 3H), 0.96 (d, J = 6.3 Hz, 3H); HRMS (ESI): *m*/*z* calcd for $C_{19}H_{27}N_2O_4$ $[M + H]^+$ 347.1971, found 347.1958.

4.6.6. (S)-tert-Butyl 2-(5-chloro-1H-indole-2-carboxamido)-4-methylpentanoate (**13f**)

Yield 72% from **12** with 5-chloro-1*H*-indole-2-carboxylic acid (**8f**); white solid; ^{1}H NMR (400 MHz, $CDCl_3$): δ 9.53 (s, 1H), 7.59 (s, 1H), 7.32 (d, J = 8.7 Hz, 1H), 7.22 (dd, J = 8.7, 1.9 Hz, 1H), 6.86–6.82 (m, 2H), 4.78–4.72 (m, 1H), 1.78–1.61 (m, 3H), 1.51 (s, 9H), 1.00 (t, J = 6.2 Hz, 6H); HRMS (ESI): *m*/*z* calcd for $C_{19}H_{26}ClN_2O_3$ $[M + H]^+$ 365.1632, found 365.1631.

4.6.7. (S)-tert-Butyl 2-(6-methoxy-1H-indole-2-carboxamido)-4-methylpentanoate (**13g**)

Yield 67% from **12** with 6-methoxy-1*H*-indole-2-carboxylic acid (**8g**); white solid; ^{1}H NMR (400 MHz, $CDCl_3$): δ 9.14 (br s, 1H), 7.50 (d, J = 8.7 Hz, 1H), 6.85–6.82 (m, 2H), 6.81 (dd, J = 8.7, 2.3 Hz, 1H), 6.59 (d, J = 8.4 Hz, 1H), 4.78–4.71 (m, 1H), 3.86 (s, 3H), 1.80–1.62 (m, 3H), 1.49 (s, 9H), 0.99 (t, J = 6.3 Hz, 6H); HRMS (ESI): *m*/*z* calcd for $C_{20}H_{29}N_2O_4$ $[M + H]^+$ 361.2127, found 361.2123.

4.6.8. (S)-tert-Butyl 2-(4-methoxy-1H-indole-2-carboxamido)-4-methylpentanoate (**13h**)

Yield 69% from **12** with 4-methoxy-1*H*-indole-2-carboxylic acid (**8h**); white solid; ^{1}H NMR (400 MHz, $CDCl_3$): δ 9.11 (br s, 1H), 7.20 (t, J = 8.0 Hz, 1H), 7.04–7.01 (m, 2H), 6.55 (br d, 1H), 6.51 (d, J = 8.0 Hz, 1H), 4.76–4.68 (m, 1H), 3.96 (s, 3H), 1.79–1.61 (m, 3H), 1.49 (s, 9H), 0.99 (t, J = 5.7 Hz, 6H); HRMS (ESI): *m*/*z* calcd for $C_{20}H_{29}N_2O_4$ $[M + H]^+$ 361.2127, found 361.2125.

4.6.9. (S)-tert-Butyl 2-(4-isopropoxy-1H-indole-2-carboxamido)-4-methylpentanoate (**13i**)

Yield 72% from **12** with 4-isopropoxy-1*H*-indole-2-carboxylic acid (**8i**); viscous oil; ^{1}H NMR (400 MHz, $CDCl_3$): δ 8.98 (br s, 1H), 7.17 (t, J = 8.0 Hz, 1H), 7.05 (s, 1H), 6.98 (d, J = 8.2 Hz, 1H), 6.56–6.50 (m, 2H), 4.76–4.70 (m, 1H), 3.49 (s, 1H), 1.76–1.62 (m, 3H), 1.49 (s, 9H), 1.42–1.41 (m, 6H), 0.99 (t, J = 6.2 Hz, 6H); HRMS (ESI): *m*/*z* calcd for $C_{22}H_{33}N_2O_4$ $[M + H]^+$ 389.2440 found 389.2447.

4.6.10. (S)-tert-Butyl 2-(4-isobutoxy-1H-indole-2-carboxamido)-4-methylpentanoate (**13j**)

Yield 70% from **12** with 4-isobutoxy-1*H*-indole-2-carboxylic acid (**8j**); yellow solid; ^{1}H NMR (400 MHz, $CDCl_3$): δ 9.09 (br s, 1H), 7.18 (t, J = 8.0 Hz, 1H), 7.06 (s, 1H), 7.00 (d, J = 8.3 Hz, 1H), 6.49 (d, J = 7.8 Hz, 1H), 4.77–4.73 (m, 1H), 3.87 (d, J = 6.5 Hz, 2H), 2.23–2.15 (m, 1H), 1.80–1.62 (m, 3H), 1.50 (s, 9H), 1.11 (s, 3H), 1.09 (s, 3H), 0.99 (t, J = 5.8 Hz, 6H); HRMS (ESI): *m*/*z* calcd for $C_{23}H_{35}N_2O_4$ $[M + H]^+$ 403.2597, found 403.2613.

4.6.11. (S)-tert-Butyl 2-(4-hydroxy-1H-indole-2-carboxamido)-4-methylpentanoate (**13k**)

Yield 55% from **12** with 4-hydroxy-1*H*-indole-2-carboxylic acid (**8k**); yellow solid; ^{1}H NMR (400 MHz, $CDCl_3$): δ 9.06 (br s, 1H), 7.23 (s, 1H), 7.11 (t, J = 7.8 Hz, 1H), 6.97 (d, J = 8.3 Hz, 1H), 6.82 (d, J = 8.9 Hz, 1H), 6.50 (d, J = 7.5 Hz, 1H), 4.85–4.76 (m, 1H), 1.76–1.62 (m, 3H), 1.53 (s, 9H), 1.00–0.94 (m, 6H); HRMS (ESI): *m*/*z* calcd for $C_{19}H_{26}N_2O_4Na$ $[M + Na]^+$ 369.1790, found 369.1783.

4.6.12. (S)-tert-Butyl 2-(5-methoxy-3-methyl-1H-indole-2-carboxamido)-4-methylpentanoate (**13l**)

Yield 63% from **12** with 5-methoxy-3-methyl-1*H*-indole-2-carboxylic acid (**8l**); yellow solid; ^{1}H NMR (400 MHz, $CDCl_3$): δ 8.83 (br s, 1H), 7.27–7.25 (m, 1H merged with $CDCl_3$), 7.02–6.99 (m, 1H), 6.95 (dd, J = 8.9, 2.4 Hz, 1H), 6.54 (d, J = 8.0 Hz, 1H), 4.80–4.73 (m, 1H), 3.88 (s, 3H), 2.60 (s, 3H), 1.80–1.63 (m, 3H), 1.51 (s, 9H), 1.00 (t, J = 6.3 Hz, 6H); HRMS (ESI): *m*/*z* calcd for $C_{21}H_{30}N_2O_4Na$ $[M + Na]^+$ 397.2103 found 397.2097.

4.6.13. (S)-tert-Butyl 2-(3-ethyl-5-methoxy-1H-indole-2-carboxamido)-4-methylpentanoate (**13m**)

Yield 65% from **12** with 3-ethyl-5-methoxy-1*H*-indole-2-carboxylic acid (**8m**); yellow solid; ^{1}H NMR (400 MHz, $CDCl_3$): δ 8.92 (br s, 1H), 7.29–7.25 (m, 1H merged with $CDCl_3$), 7.02–7.00 (m, 1H), 6.96 (dd, J = 8.9, 2.5 Hz, 1H), 6.58 (d, J = 8.0 Hz, 1H), 4.80–

4.74 (m, 1H), 3.87 (s, 3H), 3.08–2.97 (m, 2H), 1.80–1.64 (m, 3H), 1.50 (s, 9H), 1.38 (t, $J = 7.7$ Hz, 3H), 1.00 (t, $J = 5.9$ Hz, 6H); HRMS (ESI): m/z calcd for $C_{22}H_{32}N_2O_4Na$ $[M + Na]^+$ 411.2260, found 411.2260.

4.6.14. (S)-tert-Butyl 2-(1H-benzo[d]imidazole-2-carboxamido)-4-methylpentanoate (**13n**)

Yield 74% from **12** with 1*H*-benzo[*d*]imidazole-2-carboxylic acid (**8n**); white solid; ^{1}H NMR (400 MHz, $CDCl_3$): δ 11.3 (br s, 1H), 7.91 (d, $J = 8.8$ Hz, 1H), 7.82 (d, $J = 7.9$ Hz, 1H), 7.58 (d, $J = 7.2$ Hz, 1H), 7.40–7.30 (m, 2H), 4.80–4.72 (m, 1H), 1.82–1.64 (m, 3H), 1.49 (s, 9H), 1.02–0.98 (m, 6H); HRMS (ESI): m/z calcd for $C_{18}H_{26}N_3O_3$ $[M + H]^+$ 332.1974, found 332.1980.

4.6.15. (S)-tert-Butyl 2-(benzo[d]thiazole-2-carboxamido)-4-methylpentanoate (**13o**)

Yield 45% from **12** with benzo[*d*]thiazole-2-carboxylic acid (**8o**); white viscous oil; ^{1}H NMR (400 MHz, $CDCl_3$): δ 8.09 (d, $J = 8.1$ Hz, 1H), 7.96 (d, $J = 8.0$ Hz, 1H), 7.82 (d, $J = 8.7$ Hz, 1H), 7.55 (t, $J = 7.1$ Hz, 1H), 7.49 (t, $J = 7.0$ Hz, 1H), 4.78–4.71 (m, 1H), 1.80–1.66 (m, 3H), 1.50 (s, 9H), 1.02–0.98 (m, 6H); HRMS (ESI): m/z calcd for $C_{18}H_{25}N_3O_3S$ $[M + H]^+$ 349.1586, found 349.1596.

4.6.16. tert-Butyl 2-(indoline-2-carboxamido)-4-methylpentanoate (**13p**)

Yield 69% from **12** with indoline-2-carboxylic acid (**8p**); white solid; ^{1}H NMR (400 MHz, $CDCl_3$): δ 7.41 (br d, 1H), 7.31 (br d, 1H), 7.13–7.04 (m, 2H), 6.83–6.76 (m, 1H), 6.75–6.72 (m, 1H), 4.60–4.40 (m, 2H), 3.63–3.50 (m, 1H), 3.15–3.00 (m, 1H), 1.75–1.64 (m, 3H), 1.42 (s, 9H), 1.01–0.98 (m, 6H); HRMS (ESI): m/z calcd for $C_{19}H_{29}N_2O_3$ $[M + H]^+$ 333.2178, found 333.2174.

4.6.17. (S)-tert-Butyl 2-(benzofuran-2-carboxamido)-4-methylpentanoate (**13q**)

Yield 81% from **12** with benzofuran-2-carboxylic acid (**8q**); white solid; ^{1}H NMR (400 MHz, $CDCl_3$): δ 7.67 (d, $J = 7.8$ Hz, 1H), 7.51 (d, $J = 8.3$ Hz, 1H), 7.47 (s, 1H), 7.42 (t, $J = 7.7$ Hz, 1H), 7.29 (t, $J = 7.7$ Hz, 1H), 7.04 (d, $J = 8.5$ Hz, 1H), 4.80–4.71 (m, 1H), 1.80–1.60 (m, 3H), 1.50 (s, 9H), 1.00 (t, $J = 6.3$ Hz, 6H); HRMS (ESI): m/z calcd for $C_{19}H_{26}NO_4$ $[M + H]^+$ 332.1862, found 332.1857.

4.6.18. (S)-tert-Butyl 2-(1H-indole-3-carboxamido)-4-methylpentanoate (**13r**)

Yield 87% from **12** from 1*H*-indole-3-carboxylic acid (**8r**); white solid; ^{1}H NMR (400 MHz, $CDCl_3$): δ 8.19 (br s, 1H), 7.57 (d, $J = 7.5$ Hz, 1H), 7.39 (d, $J = 8.1$ Hz, 1H), 7.26–7.12 (m, 3H), 5.98 (br d, 1H), 4.55–4.48 (m, 1H), 1.52–1.30 (m, 3H), 1.37 (s, 9H), 0.86–0.80 (m, 6H); HRMS (ESI): m/z calcd for $C_{19}H_{27}N_2O_3$ $[M + H]^+$ 331.2022, found 331.2028.

4.7. General synthetic procedure for the preparation of **14a–r**

To a solution of the corresponding *tert*-butyl ester **13** (2 mmol) in CH_2Cl_2 (2 mL) at 0 °C was added TFA/H_2O (10:1, 3 mL). After 5 min stirring, the reaction mixture was allowed to stir at room temperature for 1 h. The solvent was completely evaporated under reduced pressure to give the corresponding acids **14**, which were directly used in the subsequent step without further characterization.

4.8. Synthetic procedure for the preparation of tert-butyl ((S)-1-(benzo[d]thiazol-2-yl)-1-oxo-3-((S)-2-oxopyrrolidin-3-yl)propan-2-yl) carbamate (**18**)

Compound **16** was prepared through sequential reactions from the intermediate **15**, as reported previously [12–14].

To a solution containing the acid **16** (0.540 g, 1.8 mmol) in DMF (30 mL) were added EDC·HCl (0.418 g, 2.1 mmol), HOBt·H_2O (0.334 g, 2.1 mmol), and *N*,*O*-dimethylhydroxylamine (0.213 g, 2.1 mmol) at room temperature. The solution was cooled to 0 °C, and TEA (0.304 mL, 2.1 mmol) was then added slowly. After 2 h, the DMF was evaporated, and the resulting residue was dissolved in ethyl acetate (100 mL). The organic phase was subsequently washed with 5% citric acid (20 mL × 2), 5% $NaHCO_3$ (20 mL × 2), and brine (50 mL). The organic layer was then dried over Na_2SO_4 and concentrated under reduced pressure to yield the Weinreb amide derivative **17**, which was purified by column chromatography (EtOAc/MeOH = 9.5:0.5).

To a solution of benzothiazole (10.0 mmol) in THF (20 mL) at −78 °C was added *n*-BuLi (2.0 M in THF, 1.67 mL) dropwise over 20 min. After 1 h stirring, the Weinreb amide **17** (0.640 g, 2.0 mmol) in THF (10 mL) was slowly added over 10 min, and the solution was stirred for 3 h. The reaction was quenched with sat. NH_4Cl and allowed to stir at 0 °C for 20 min. The mixture was evaporated and dissolved in EtOAc (100 mL). This solution was washed with water (50 mL) and brine (40 mL), and then dried over Na_2SO_4. The organic layer was concentrated under reduced pressure, and the resulting residue was subjected to flash chromatography (EtOAc/MeOH = 9:1) to obtain the pure compound **18**.

The characterization data for the compounds **17** and **18** are reported elsewhere [12–14].

4.8.1. Synthetic procedure for the preparation of N-((S)-1-(((S)-1-(benzo[d]thiazol-2-yl)-1-oxo-3-((S)-2-oxopyrrolidin-3-yl)propan-2-yl)amino)-4-methyl-1-oxopentan-2-yl)-5-oxopyrrolidine-2-carboxamide (**5a**)

To a solution of **18** (0.200 g, 0.5 mmol) in CH_2Cl_2 (3 mL) at 0 °C was added TFA/H_2O (10:1, 2 mL), and the solution was stirred for 1 h. After evaporating the solvent under reduced pressure, the corresponding deprotected lactam residue (0.100 g, 0.53 mmol) was coupled to the carboxylic acid **14a** (0.136 g, 0.38 mmol) using the coupling agent HBTU (0.147 g, 0.38 mmol) in the presence of diisopropylethylamine (0.050 mL, 0.38 mmol) in DMF (3 mL) at 0 °C. After 5 min stirring, the ice bath was removed, and the solution was allowed to stir for 2 h under ambient conditions. The solvent was then evaporated under high vacuum, and the residue was dissolved in ethyl acetate (50 mL). The organic layer was washed with 5% citric acid (20 mL × 2), 5% $NaHCO_3$ (20 mL × 2), and brine (25 mL). The solution was dried over Na_2SO_4, filtered, and evaporated under reduced pressure to give compound **5a**. Yield 43%; white solid; ^{1}H NMR (400 MHz, CD_3OD): δ 8.20 (d, $J = 8.4$ Hz, 1H), 8.12 (d, $J = 7.8$ Hz, 1H), 7.68–7.55 (m, 2H), 5.75–5.65 (m, 1H), 4.50–4.40 (m, 1H), 4.30–4.20 (m, 1H), 3.40–3.28 (m, 2H merged with CD_3OD), 2.80–2.60 (m, 1H), 2.59–2.18 (m, 5H), 2.17–2.01 (m, 2H), 2.00–1.75 (m, 1H), 1.74–1.40 (m, 3H), 1.00–0.86 (m, 6H); ^{13}C NMR (400 MHz, CD_3OD): δ 193.5, 182.0, 181.6, 175.1, 165.5, 154.8, 138.4, 129.3, 128.5, 126.5, 123.7, 58.3, 55.7, 53.3, 41.7, 40.3, 39.5, 33.6, 30.0, 29.1, 26.8, 26.5, 25.9, 23.3, 21.9; HRMS (ESI): m/z calcd for $C_{25}H_{32}N_5O_5S$ $[M + H]^+$ 514.2124 found 514.2115.

The compounds **5b–r** was synthesized from **18** with the **14b–r** using a procedure similar to that described for the preparation of **5a**.

4.8.2. N-((S)-1-(((S)-1-(Benzo[d]thiazol-2-yl)-1-oxo-3-((S)-2-oxopyrrolidin-3-yl)propan-2-yl)amino)-4-methyl-1-oxopentan-2-yl)-1H-pyrrole-2-carboxamide (**5b**)

Yield 38%; white solid; ^{1}H NMR (400 MHz, CD_3OD): δ 8.14–8.05 (m, 2H), 7.62–7.54 (m, 2H), 6.95–6.85 (m, 2H), 6.18–6.15 (m, 2H), 5.72–5.65 (m, 1H), 4.70–4.42 (m, 1H), 3.36–3.10 (m, 2H merged with CD_3OD), 2.80–2.56 (m, 1H), 2.54–2.40 (m, 1H), 2.39–2.20 (m, 1H), 2.19–1.99 (m, 2H), 1.98–1.60 (m, 3H), 1.00–0.85 (m, 6H); ^{13}C NMR (400 MHz, CD_3OD): δ 193.5, 181.8, 175.6, 165.4, 163.5, 154.7, 138.3, 129.3, 128.4, 126.5, 126.4, 123.7, 123.3, 112.8, 110.3, 55.6, 53.1,

41.9, 41.6, 40.0, 34.0, 28.8, 26.0, 23.4, 22.1; HRMS (ESI): *m/z* calcd for $C_{25}H_{30}N_5O_4S$ $[M + H]^+$ 496. 2019 found 496. 2011.

*4.8.3. N-((S)-1-(((S)-1-(Benzo[d]thiazol-2-yl)-1-oxo-3-((S)-2-oxopyrrolidin-3-yl)propan-2-yl)amino)-4-methyl-1-oxopentan-2-yl)-1H-indole-2-carboxamide (**5c**)*

Yield 51%; light yellow solid; ^{1}H NMR (400 MHz, CD_3OD): δ 8.10–8.06 (m, 2H), 7.63–7.54 (m, 3H), 7.47–7.38 (m, 1H), 7.23–7.15 (m, 2H), 7.14–7.04 (m, 1H), 5.70–5.67 (m, 1H), 4.75–4.68 (m, 1H), 3.49–3.29 (m, 2H), 2.78–2.62 (m, 1H), 2.61–2.41 (m, 1H), 2.39–2.24 (m, 1H), 2.23–2.03 (m, 2H), 2.02–1.72 (m, 3H), 0.98–0.88 (m, 6H); ^{13}C NMR (400 MHz, CD_3OD): δ 193.4, 181.8, 175.4, 165.4, 164.0, 154.7, 138.2, 131.6, 129.2, 128.9, 128.4, 126.4, 125.2, 123.6, 122.2, 121.2, 113.0, 105.3, 55.7, 53.4, 41.8, 41.5, 40.0, 33.9, 28.8, 26.0, 23.3, 22.1; HRMS (ESI): *m/z* calcd for $C_{29}H_{32}N_5O_4S$ $[M + H]^+$ 546.2175 found 546.2157.

*4.8.4. N-((S)-1-(((S)-1-(Benzo[d]thiazol-2-yl)-1-oxo-3-((S)-2-oxopyrrolidin-3-yl)propan-2-yl)amino)-4-methyl-1-oxopentan-2-yl)-5-methoxy-1H-indole-2-carboxamide (**5d**)*

Yield 46%; light yellow solid; ^{1}H NMR (400 MHz, $CDCl_3$): δ 8.10–8.06 (m, 1H), 8.00–7.96 (m, 1H), 7.56–7.48 (m, 2H), 7.07–7.00 (m, 2H), 6.96–6.92 (m, 2H), 5.82–5.68 (m, 1H), 4.80–4.75 (m, 1H), 3.85 (s, 3H), 3.44–3.26 (m, 2H), 2.70–2.42 (m, 2H), 2.41–2.14 (m, 1H), 2.13–1.90 (m, 2H), 1.89–1.64 (m, 3H), 0.98–0.88 (m, 6H); ^{13}C NMR (400 MHz, CD_3OD): δ 193.5, 181.8, 175.4, 165.6, 164.0, 155.8, 154.7, 138.3, 133.8, 132.0, 129.2, 128.3, 127.1, 126.4, 123.6, 116.7, 113.9, 105.2, 103.2, 56.2, 55.7, 53.4, 41.5, 40.0, 33.9, 29.3, 28.8, 26.1, 23.4, 22.0; HRMS (ESI): *m/z* calcd for $C_{30}H_{34}N_5O_5S$ $[M + H]^+$ 576.2281 found 576.2294.

*4.8.5. N-((S)-1-(((S)-1-(Benzo[d]thiazol-2-yl)-1-oxo-3-((S)-2-oxopyrrolidin-3-yl)propan-2-yl)amino)-4-methyl-1-oxopentan-2-yl)-5-hydroxy-1H-indole-2-carboxamide (**5e**)*

Yield 37%; light yellow solid; ^{1}H NMR (400 MHz, CD_3OD): δ 8.08–8.04 (m, 2H), 7.57–7.50 (m, 2H), 7.30–7.23 (m, 1H), 7.02–6.93 (m, 2H), 6.81 (dd, J = 8.9, 2.3 Hz, 1H), 5.70–5.65 (m, 1H), 4.75–4.65 (m, 1H), 3.40–3.21 (m, 2H merged with CD_3OD), 2.80–2.60 (m, 1H), 2.59–2.40 (m, 1H), 2.39–2.22 (m, 1H), 2.21–1.93 (m, 2H), 1.92–1.62 (m, 3H), 1.00–0.90 (m, 6H); ^{13}C NMR (400 MHz, CD_3OD): δ 193.4, 175.4, 165.6, 165.4, 164.0, 154.7, 152.3, 138.2, 133.5, 132.7, 129.6, 128.4, 128.3, 126.5, 123.6, 116.2, 113.6, 105.8, 104.6, 55.7, 53.4, 41.8, 41.6, 40.0, 34.0, 28.8, 26.1, 23.3, 22.1; HRMS (ESI): *m/z* calcd for $C_{29}H_{32}N_5O_5S$ $[M + H]^+$ 562.2124 found 562.2133.

*4.8.6. N-((S)-1-(((S)-1-(Benzo[d]thiazol-2-yl)-1-oxo-3-((S)-2-oxopyrrolidin-3-yl)propan-2-yl)amino)-4-methyl-1-oxopentan-2-yl)-5-chloro-1H-indole-2-carboxamide (**5f**)*

Yield 41%; white solid; ^{1}H NMR (400 MHz, CD_3OD): δ 8.00–7.93 (m, 2H), 7.50–7.40 (m, 3H), 7.28 (t, J = 8.0 Hz, 1H), 7.06 (dd, J = 8.8, 2.0 Hz, 1H), 7.05–6.97 (m, 1H), 5.62–5.56 (m, 1H), 4.65–4.55 (m, 1H), 3.30–3.12 (m, 2H merged with CD_3OD), 2.70–2.62 (m, 1H), 2.52–2.30 (m, 2H), 2.29–2.13 (m, 1H), 2.11–1.83 (m, 2H), 1.82–1.55 (m, 2H), 0.90–0.80 (m, 6H); ^{13}C NMR (400 MHz, CD_3OD): δ 193.5, 181.8, 175.3, 165.6, 163.5, 154.7, 138.3, 136.6, 133.2, 129.8, 128.4, 128.3, 126.7, 125.3, 123.6, 121.9, 114.4, 104.7, 104.6, 55.6, 53.4, 41.8, 41.5, 40.0, 33.9, 28.8, 26.0, 23.3, 22.1; HRMS (ESI): *m/z* calcd for $C_{29}H_{31}ClN_5O_4S$ $[M + H]^+$ 580.1785 found 580.1795.

*4.8.7. N-((S)-1-(((S)-1-(Benzo[d]thiazol-2-yl)-1-oxo-3-((S)-2-oxopyrrolidin-3-yl)propan-2-yl)amino)-4-methyl-1-oxopentan-2-yl)-6-methoxy-1H-indole-2-carboxamide (**5g**)*

Yield 38%; white solid; ^{1}H NMR (400 MHz, $CDCl_3$): δ 8.97 (br d, 1H), 8.72 (br d, 1H), 8.18–8.06 (m, 1H), 8.00–7.92 (m, 1H), 7.58–7.44 (m, 2H), 7.00–6.79 (m, 1H), 6.78–6.75 (m, 1H), 6.40–6.25 (m, 1H), 5.85–5.68 (m, 1H), 4.93–4.80 (m, 1H), 3.87 (s, 3H), 3.39–3.13 (m, 2H), 2.70–2.55 (m, 1H), 2.54–2.40 (m, 1H), 2.39–2.29 (m, 1H), 2.28–2.04 (m, 2H), 2.03–1.92 (m, 1H), 1.90–1.66 (m, 3H), 0.96–0.80 (m, 6H); ^{13}C NMR (400 MHz, CD_3OD): δ 193.4, 181.5, 175.6, 165.2, 164.1, 159.6, 155.9, 139.4, 138.9, 130.5, 129.2, 128.4, 126.4, 123.6 (2 carbons), 123.2, 112.7, 105.8, 94.8, 55.8, 55.7, 53.3, 41.8, 41.5, 40.0, 34.0, 28.8, 26.0, 23.3, 22.1; HRMS (ESI): *m/z* calcd for $C_{30}H_{34}N_5O_5S$ $[M + H]^+$ 576.2281 found 576.2268.

*4.8.8. N-((S)-1-(((S)-1-(Benzo[d]thiazol-2-yl)-1-oxo-3-((S)-2-oxopyrrolidin-3-yl)propan-2-yl)amino)-4-methyl-1-oxopentan-2-yl)-4-methoxy-1H-indole-2-carboxamide (**5h**)*

Yield 45%; light yellow solid; ^{1}H NMR (400 MHz, $CDCl_3$): δ 9.65 (br s, 1H), 8.89 (br s, 1H), 8.57 (br s, 1H), 8.08–8.06 (m, 1H), 7.98–7.94 (m, 1H), 7.56–7.49 (m, 2H), 7.25–6.81 (m, 4H), 6.75–6.43 (m, 1H), 5.99–5.60 (m, 1H), 5.00–4.80 (m, 1H), 3.92 (s, 3H), 3.45–3.10 (m, 2H), 2.98–1.64 (m, 8H), 0.99–0.83 (m, 6H); ^{13}C NMR (400 MHz, CD_3OD): δ 193.4, 181.7, 175.3, 165.4, 164.0, 154.7, 152.8, 140.3, 138.2, 130.1, 129.2, 128.4, 126.49, 126.43, 123.6, 119.6, 104.8, 104.5, 103.7, 55.7, 53.4, 41.8, 41.5, 40.0, 34.0, 30.6, 28.8, 26.0, 23.3, 22.1; HRMS (ESI): *m/z* calcd for $C_{30}H_{34}N_5O_5S$ $[M + H]^+$ 576.2281 found 576.2264.

*4.8.9. N-((S)-1-(((S)-1-(Benzo[d]thiazol-2-yl)-1-oxo-3-((S)-2-oxopyrrolidin-3-yl)propan-2-yl)amino)-4-methyl-1-oxopentan-2-yl)-4-isopropoxy-1H-indole-2-carboxamide (**5i**)*

Yield 49%; light yellow solid; ^{1}H NMR (400 MHz, CD_3OD): δ 8.07–8.01 (m, 2H), 7.56–7.44 (m, 2H), 7.34–7.25 (m, 1H), 7.20–7.09 (m, 1H), 7.07–6.95 (m, 1H), 6.60–6.48 (m, 1H), 5.72–5.62 (m, 1H), 4.78–4.60 (m, 2H), 3.40–3.18 (m, 2H), 2.80–2.65 (m, 1H), 2.64–2.40 (m, 1H), 2.39–2.20 (m, 1H), 2.19–2.00 (m, 2H), 1.99–1.62 (m, 3H), 1.40–1.27 (m, 6H), 0.99–0.83 (m, 6H); ^{13}C NMR (400 MHz, CD_3OD): δ 193.4, 181.8, 175.4, 165.4, 164.0, 154.6, 153.7, 140.1, 138.2, 130.2, 129.2, 128.3, 126.4, 126.2, 123.6, 121.3, 106.0, 103.36, 103.32, 71.1, 55.7, 53.4, 41.8, 41.5, 40.0, 34.0, 28.7, 26.0, 23.4, 22.5 (2 carbons), 22.1; HRMS (ESI): *m/z* calcd for $C_{32}H_{38}N_5O_5S$ $[M + H]^+$ 604.2594 found 604.2603.

*4.8.10. N-((S)-1-(((S)-1-(Benzo[d]thiazol-2-yl)-1-oxo-3-((S)-2-oxopyrrolidin-3-yl)propan-2-yl)amino)-4-methyl-1-oxopentan-2-yl)-4-isobutoxy-1H-indole-2-carboxamide (**5j**)*

Yield 52%; light yellow solid; ^{1}H NMR (400 MHz, CD_3OD): δ 8.04–8.00 (m, 2H), 7.52–7.44 (m, 2H), 7.35–7.20 (m, 1H), 7.10 (t, J = 8.0 Hz, 1H), 7.01–6.97 (m, 1H), 6.50–6.42 (m, 1H), 5.75–5.65 (m, 1H), 4.75–4.65 (m, 1H), 3.87–3.82 (m, 2H), 3.40–3.20 (m, 2H), 2.76–2.47 (m, 1H), 2.45–2.28 (m, 2H), 2.27–2.15 (m, 1H), 2.14–2.00 (m, 2H), 1.99–1.65 (m, 3H), 1.09–1.06 (m, 6H), 0.99–0.83 (m, 6H); ^{13}C NMR (400 MHz, CD_3OD): δ 193.4, 181.8, 175.5, 165.4, 164.0, 155.1, 154.6, 139.8, 138.2, 130.1, 129.2, 128.3, 126.4, 126.3, 123.6, 120.3, 106.0, 103.1, 101.2, 75.3, 55.7, 53.4, 41.8, 41.5, 40.0, 34.1, 29.7, 28.7, 26.0, 23.4, 22.1, 19.7 (2 carbons); HRMS (ESI): *m/z* calcd for $C_{33}H_{40}N_5O_5S$ $[M + H]^+$ 618.2750 found 618.2767.

*4.8.11. N-((S)-1-(((S)-1-(Benzo[d]thiazol-2-yl)-1-oxo-3-((S)-2-oxopyrrolidin-3-yl)propan-2-yl)amino)-4-methyl-1-oxopentan-2-yl)-4-hydroxy-1H-indole-2-carboxamide (**5k**)*

Yield 51%; white solid; ^{1}H NMR (400 MHz, CD_3OD): δ 8.00–7.95 (m, 2H), 7.50–7.38 (m, 2H), 7.24–7.12 (m, 1H), 6.97–6.91 (m, 1H), 6.85–6.78 (m, 1H), 6.31 (d, J = 7.6 Hz, 1H) 5.62–5.54 (m, 1H), 4.62–4.55 (m, 1H), 3.35–3.10 (m, 2H merged with CD_3OD), 2.70–2.53 (m, 1H), 2.51–2.21 (m, 2H), 2.20–2.12 (m, 2H), 2.10–1.83 (m, 1H), 1.82–1.58 (m, 3H), 0.90–0.82 (m, 6H); ^{13}C NMR (400 MHz, CD_3OD): δ 193.4, 181.8, 175.4, 165.4, 154.7, 152.8, 140.3, 138.2, 130.1, 129.2, 128.4, 126.5, 126.49, 126.43, 123.6, 119.6, 104.8, 104.5, 103.1, 55.7, 53.4, 41.8, 41.5, 40.0, 34.0, 28.8, 26.0, 23.3, 22.1; HRMS

(ESI): *m*/*z* calcd for $C_{29}H_{32}N_5O_5S$ [M + H]$^+$ 562.2124, found 562.2122.

*4.8.12. N-((S)-1-(((S)-1-(Benzo[d]thiazol-2-yl)-1-oxo-3-((S)-2-oxopyrrolidin-3-yl)propan-2-yl)amino)-4-methyl-1-oxopentan-2-yl)-5-methoxy-3-methyl-1H-indole-2-carboxamide (**5l**)*

Yield 46%; white solid; ^{1}H NMR (400 MHz, $CDCl_3$): δ 8.56 (br s, 1H), 7.90–7.84 (m, 1H), 7.75 (d, J = 7.8 Hz, 1H), 7.60–7.49 (m, 2H), 7.35–7.22 (m, 1H merged with $CDCl_3$), 7.14–7.11 (m, 1H), 6.99–6.87 (m, 1H), 5.75–5.65 (m, 1H), 4.90–4.81 (m, 1H), 3.86 (s, 3H), 3.49–3.34 (m, 2H), 2.70–2.59 (m, 1H), 2.58–2.29 (m, 3H), 2.47 (s, 3H), 2.28–2.12 (m, 1H), 2.08–1.91 (m, 1H), 1.93–1.67 (m, 2H), 1.03–0.88 (m, 6H); ^{13}C NMR (400 MHz, CD_3OD): δ 193.1, 181.2, 175.7, 165.4, 155.5, 152.8, 140.3, 138.2, 133.1, 129.2, 128.7, 126.4, 123.7, 122.7, 117.5, 116.9, 113.9, 101.5, 56.5, 56.0, 41.5, 40.2, 33.5, 29.4, 28.3, 25.5, 24.9, 23.4, 22.1, 18.7, 15.9; HRMS (ESI): *m*/*z* calcd for $C_{31}H_{36}N_5O_5S$ [M + H]$^+$ 590.2437 found 590.2443.

*4.8.13. N-((S)-1-(((S)-1-(Benzo[d]thiazol-2-yl)-1-oxo-3-((S)-2-oxopyrrolidin-3-yl)propan-2-yl)amino)-4-methyl-1-oxopentan-2-yl)-3-ethyl-5-methoxy-1H-indole-2-carboxamide (**5m**)*

Yield 41%; white solid; ^{1}H NMR (400 MHz, $CDCl_3$): δ 8.00–7.97 (m, 1H), 7.84–7.74 (m, 1H), 7.55–7.47 (m, 2H), 7.00–6.85 (m, 2H), 6.70–6.52 (m, 1H), 5.91–5.68 (m, 1H), 4.90–4.85 (m, 1H), 3.86 (s, 3H), 3.49–3.38 (m, 2H), 3.00–2.73 (m, 2H), 2.72–2.58 (m, 1H), 2.57–2.38 (m, 1H), 2.37–2.01 (m, 4H), 2.00–1.68 (m, 2H), 1.40–1.21 (m, 3H), 1.02–0.88 (m, 6H); HRMS (ESI): *m*/*z* calcd for $C_{32}H_{38}N_5O_5S$ [M + H]$^+$ 604.2594 found 604.2607.

*4.8.14. N-((S)-1-(((S)-1-(Benzo[d]thiazol-2-yl)-1-oxo-3-((S)-2-oxopyrrolidin-3-yl)propan-2-yl)amino)-4-methyl-1-oxopentan-2-yl)-1H-benzo[d]imidazole-2-carboxamide (**5n**)*

Yield 49%; white solid; ^{1}H NMR (400 MHz, CD_3OD): δ 8.15–8.07 (m, 2H), 7.70–7.68 (m, 2H), 7.57–7.53 (m, 2H), 7.43–7.38 (m, 2H), 5.73–5.68 (m, 1H), 4.73–4.70 (m, 1H), 3.40–3.28 (m, 2H merged with CD_3OD), 2.80–2.66 (m, 1H), 2.65–2.35 (m, 2H), 2.34–2.20 (m, 1H), 2.19–1.95 (m, 2H), 1.93–1.70 (m, 2H), 1.00–0.96 (m, 6H); HRMS (ESI): *m*/*z* calcd for $C_{28}H_{31}N_6O_4S$ [M + H]$^+$ 547.2127, found 547.2127.

*4.8.15. N-((S)-1-(((S)-1-(Benzo[d]thiazol-2-yl)-1-oxo-3-((S)-2-oxopyrrolidin-3-yl)propan-2-yl)amino)-4-methyl-1-oxopentan-2-yl)benzo[d]thiazole-2-carboxamide (**5o**)*

Yield 43%; white solid; ^{1}H NMR (400 MHz, CD_3OD): δ 8.03–7.95 (m, 4H), 7.51–7.40 (m, 4H), 5.62–5.58 (m, 1H), 4.64–4.51 (m, 1H), 3.30–3.12 (m, 2H merged with CD_3OD), 2.70–2.61 (m, 1H), 2.50–2.30 (m, 2H), 2.29–2.10 (m, 1H), 2.09–1.74 (m, 2H), 1.73–1.64 (m, 2H), 0.90–0.84 (m, 6H); ^{13}C NMR (400 MHz, CD_3OD): δ 193.3, 181.8, 174.6, 165.4, 164.3, 161.7, 154.7, 154.4, 138.3, 138.1, 129.2, 128.4, 128.2, 128.1, 126.4, 125.5, 123.7, 123.6, 55.6, 53.7, 42.1, 41.5, 40.0, 33.8, 28.7, 26.0, 23.3, 22.1; HRMS (ESI): *m*/*z* calcd for $C_{28}H_{30}N_5O_4S_2$ [M + H]$^+$ 564.1739, found 564.1741.

*4.8.16. N-((S)-1-(((S)-1-(Benzo[d]thiazol-2-yl)-1-oxo-3-((S)-2-oxopyrrolidin-3-yl)propan-2-yl)amino)-4-methyl-1-oxopentan-2-yl)indoline-2-carboxamide (**5p**)*

Yield 43%; white solid; ^{1}H NMR (400 MHz, CD_3OD): δ 8.18–8.08 (m, 2H), 7.68–7.50 (m, 2H), 7.49–7.25 (m, 1H), 7.24–7.14 (m, 2H), 7.08–6.99 (m, 1H), 5.72–5.63 (m, 1H), 4.85–4.75 (m, 1H), 4.74–4.49 (m, 1H), 3.72–3.47 (m, 1H), 3.43–3.10 (m, 1H), 2.85–2.60 (m, 2H), 2.59–2.32 (m, 2H), 2.30–2.18 (m, 1H), 2.16–2.00 (m, 2H), 1.99–1.55 (m, 3H), 1.00–0.90 (m, 6H); ^{13}C NMR (400 MHz, CD_3OD): δ 193.4, 181.8, 175.4, 165.4, 164.0, 154.7, 138.4, 138.2, 131.6, 129.2, 128.9, 128.4, 126.4, 125.2, 123.6, 122.8, 121.2, 113.0, 105.3, 55.7, 53.4, 41.8, 41.5, 40.0, 33.9, 28.8, 26.0, 23.3, 22.1; HRMS (ESI): *m*/*z* calcd for $C_{29}H_{34}N_5O_4S$ [M + H]$^+$ 548.2332 found 548.2328.

*4.8.17. N-((S)-1-(((S)-1-(Benzo[d]thiazol-2-yl)-1-oxo-3-((S)-2-oxopyrrolidin-3-yl)propan-2-yl)amino)-4-methyl-1-oxopentan-2-yl)benzofuran-2-carboxamide (**5q**)*

Yield 51%; white solid; ^{1}H NMR (400 MHz, $CDCl_3$): δ 8.09 (d, J = 7.2 Hz, 1H), 7.70–7.64 (m, 1H), 7.61–7.53 (m, 2H), 7.51–7.39 (m, 1H), 7.38–7.26 (m, 3H), 7.24–7.16 (m, 2H), 5.72–5.56 (m, 1H), 4.83–4.79 (m, 1H), 3.49–3.30 (m, 2H), 2.70–2.55 (m, 1H), 2.54–2.22 (m, 2H), 2.21–2.00 (m, 2H), 1.99–1.70 (m, 3H), 1.04–0.99 (m, 6H); HRMS (ESI): *m*/*z* calcd for $C_{29}H_{31}N_4O_5S$ [M + H]$^+$ 547.2015 found 547.2019.

*4.8.18. N-((S)-1-(((S)-1-(Benzo[d]thiazol-2-yl)-1-oxo-3-((S)-2-oxopyrrolidin-3-yl)propan-2-yl)amino)-4-methyl-1-oxopentan-2-yl)-1H-indole-3-carboxamide (**5r**)*

Yield 43%; light yellow solid; ^{1}H NMR (400 MHz, $CDCl_3$): δ 8.20–8.06 (m, 1H), 7.98 (d, J = 7.2 Hz, 1H), 7.63–7.51 (m, 2H), 7.40–7.33 (m, 1H), 7.29–7.11 (m, 4H merged with $CDCl_3$), 5.80–5.66 (m, 1H), 4.65–4.50 (m, 1H), 3.49–3.29 (m, 2H), 2.60–2.42 (m, 2H), 2.41–2.23 (m, 1H), 2.22–1.95 (m, 2H), 1.85–1.27 (m, 3H), 0.98–0.88 (m, 6H); ^{13}C NMR (400 MHz, CD_3OD): δ 193.4, 181.8, 175.4, 165.4, 164.0, 154.7, 138.4, 138.2, 131.6, 129.2, 128.9, 128.4, 126.4, 125.2, 123.6, 122.8, 121.2, 113.0, 105.3, 55.7, 53.4, 41.8, 41.5, 40.0, 33.9, 28.8, 26.0, 23.3, 22.1; HRMS (ESI): *m*/*z* calcd for $C_{29}H_{31}N_5O_4SNa$ [M + Na]$^+$ 568.1994 found 568.1990.

5. Molecular docking study

The crystal structure of the SARS-CoV 3CL^{pro} protease in complex with a substrate analog inhibitor (coded 1WOF) [27] was obtained from the Protein Data Bank (PDB; http://www.rcsb.org/pdb/home/home.do). Initially, a binding model of **5h** with 3CL^{pro} was simulated to form a basis for comparison with our previous lead **4** and substrate analogs, using molecular operating environment (MOE) software. Several minimization processes were performed using the MMFF94X force field to model the solvation environment surrounding the inhibitor. Structures having a relatively low binding free energy and a high number of cluster members were selected for the subsequent docking conformation optimization step. The minimized energies of **5h**, obtained from the docking study, were −41.49 and −37.51 kcal/mol. The substrate analog was removed from the crystal structure and the docking studies were performed using **5c**, **5q**, and **5r** according to a method similar to the method described for the **5h** docking study.

6. Isothermal titration calorimetry

The binding of **5h** was studied by isothermal titration calorimetry (ITC) using a VP-ITC microcalorimeter from MicroCal/GE Healthcare (Northampton, MA, USA). SARS-CoV 3CL^{pro} and the inhibitor were dissolved in buffer composed of 10 mM sodium phosphate, pH 7.4, 10 mM NaCl, 1 mM TCEP, and 1 mM EDTA with 2% DMSO. The titration was performed at 25 °C by injecting 10 μL aliquots of protease solution into the calorimetric cell (volume ~ 1.4 mL) containing the inhibitor at a concentration of 6 μM. The concentration of protease in the syringe was 109 μM. The heat evolved upon each injection of protease was obtained from the integral of the calorimetric signal. The heat associated with inhibitor binding was obtained by subtracting the heat of dilution from the heat of reaction. The individual heats were plotted against the molar ratio, and the enthalpy change (ΔH) and association constant ($K_a = 1/K_d$) were obtained by nonlinear regression of the data (see Fig. 4).

Acknowledgments

This research was supported by Grants from the Ministry of Education, Culture, Sports, Science and Technology (MEXT) of Japan, including a Grant-in-aid for Young Scientists (*Tokubetsu Kenkyuin Shorei-hi*) 23·01104 and a Grant-in-aid for Scientific Research 23659059. E.F. acknowledges support from the National Institutes of Health (Grants GM57144 and GM56550) and from the National Science Foundation (MCB-1157506).

Appendix A. Supplementary data

Supplementary data related to this article can be found at http://dx.doi.org/10.1016/j.ejmech.2013.07.037.

References

[1] J.-F. He, G.-W. Peng, J. Min, D.-W. Yu, W.-L. Liang, S.-Y. Zhang, R.-H. Xu, H.-Y. Zheng, X.-W. Wu, J. Xu, Z.-H. Wang, L. Fang, X. Zhang, H. Li, X.-G. Yan, J.-H. Lu, Z.-H. Hu, J.-C. Huang, Z.-Y. Wan, J.-L. Hou, J.-Y. Lin, H.-D. Song, S.-Y. Wang, X.-J. Zhou, G.-W. Zhang, B.-W. Gu, H.-J. Zheng, X.-L. Zhang, M. He, K. Zheng, B.-F. Wang, G. Fu, X.-N. Wang, S.-J. Chen, Z. Chen, P. Hao, H. Tang, S.-X. Ren, Y. Zhong, Z.-M. Guo, Q. Liu, Y.-G. Miao, X.-Y. Kong, W.-Z. He, Y.-X. Li, C.-I. Wu, G.-P. Zhao, R.W.K. Chiu, S.S.C. Chim, Y.-K. Tong, P.K.S. Chan, J.S. Tam, Y.M.D. Lo, Science 303 (2004) 1666–1669.

[2] T.G. Ksiazek, D. Erdman, C.S. Goldsmith, S.R. Zaki, T. Peret, S. Emery, S. Tong, C. Urbani, J.A. Comer, W. Lim, P.E. Rollin, S.F. Dowell, A.-E. Ling, C.D. Humphrey, W.-J. Shieh, J. Guarner, C.D. Paddock, P. Rota, B. Fields, J. DeRisi, J.-Y. Yang, N. Cox, J.M. Hughes, J.W. LeDuc, W.J. Bellini, L.J. Anderson, N. Engl. J. Med. 348 (2003) 1953–1966.

[3] C. Drosten, S. Guenther, W. Preiser, S. Van Der Werf, H.-R. Brodt, S. Backer, H. Rabenau, M. Panning, L. Kolesnikova, R.A.M. Fouchier, A. Berger, A.-M. Burguiére, J. Cinatl, M. Eickmann, N. Escriou, K. Grywna, S. Kramme, J.-C. Manuguerra, S. Mueller, V. Rickerts, M. Stuermer, S. Vieth, H.-D. Klenk, A.D.M.E. Osterhaus, H. Schmitz, H.W.N. Doerr, N. Engl. J. Med. 348 (2003) 1967–1977.

[4] K. Pyrc, B. Berkhout, L. Van der Hoek, J. Virol. 81 (2007) 3051–3057.

[5] B.C. Fielding, Future Microbiol. 6 (2011) 153–159.

[6] L.-J. Cui, C. Zhang, T. Zhang, R.-J. Lu, Z.-D. Xie, L.-L. Zhang, C.-Y. Liu, W.-M. Zhou, X.-J. Ma, W.-J. Tan, Adv. Virol. (2011). No. 129134.

[7] A.M. Zaki, S. van Boheemen, T.M. Bestebroer, A.D.M.E. Osterhaus, R.A.M. Fouchier, N. Engl. J. Med. 367 (2012) 1814–1820.

[8] http://www.independent.co.uk/life-style/health-and-families/health-news/sarslike-virus-spreads-persontoperson-in-the-uk-8492750.html.

[9] P.A. Rota, M.S. Oberste, S.S. Monroe, W.A. Nix, R. Campagnoli, J.P. Icenogle, S. Penaranda, B. Bankamp, K. Maher, M.H. Chem, S. Tong, A. Tamin, L. Lowe, M. Frace, J.L. DeRisi, Q. Chen, D. Wang, D.D. Erdman, T.C. Peret, C. Burns, T.G. Ksiazek, P.E. Rollin, A. Sanchez, S. Liffick, B. Holloway, J. Limor, K. McCaustland, M. Olsen-Rasmussen, R. Fouchier, S. Günther, A.D. Osterhaus, C. Drosten, M.A. Pallansch, L.J. Anderson, W.J. Bellini, Science 300 (2003) 1394–1399.

[10] K. Anand, J. Ziebuhr, P. Wadhwani, J.R. Mesters, R. Hilgenfeld, Science 300 (2003) 1763–1767.

[11] E.J. Snijder, P.J. Bredenbeek, J.C. Dobbe, V. Thiel, J. Ziebuhr, L.L.M. Poon, Y. Guan, M. Rozanov, W.J. Spaan, A.E. Gorbalenya, J. Mol. Biol. 331 (2003) 991–1004.

[12] (a) M.O. Sydnes, Y. Hayashi, V.K. Sharma, T. Hamada, U. Bacha, J. Barrila, E. Freire, Y. Kiso, Tetrahedron 62 (2006) 8601–8609;
(b) T. Regnier, D. Sarma, K. Hidaka, U. Bacha, E. Freire, Y. Hayashi, Y. Kiso, Bioorg. Med. Chem. Lett. 19 (2009) 2722–2727.

[13] S. Konno, P. Thanigaimalai, T. Yamamoto, K. Nakada, Y.R. Kakiuchi, K. Takayama, Y. Yamazaki, F. Yakushiji, K. Akaji, Y. Kiso, Y. Kawasaki, S.H. Chen, E. Freire, Y. Hayashi, Bioorg. Med. Chem. 21 (2013) 412–424.

[14] P. Thanigaimalai, S. Konno, T. Yamamoto, Y. Koiwai, A. Taguchi, K. Takayama, F. Yakushiji, K. Akaji, Y. Kiso, Y. Kawasaki, S-E. Chen, A. Naser-Tavakolian, A. Schön, E. Freire, Y. Hayashi, Eur. J. Med. Chem. 65 (2013) 436–447.

[15] R. Hersperger, P. Janser, E. Pfenninger, H.J. Wuethrich, W. Miltz, From PCT Int. Appl., 2005077932, 25 August 2005.

[16] K.X. Chen, S. Venkatraman, F.G. Njoroge, S.B. Rosenblum, C.A. Lesburg, J.S. Duca, N.-Y. Shih, F. Velazquez, G.N. Anilkumar, Q. Zeng, J.A. Kozlowski, From PCT Int. Appl., WO 2008082484 A1 20080710, 2008.

[17] N.M. Gray, M.S. Dappen, B.K. Cheng, A.A. Cordi, J.P. Biesterfeldt, W.F. Hood, J.B. Monahan, J. Med. Chem. 34 (1991) 1283–1292.

[18] J.H. Lee, J.-H. So, J.H. Jeong, E.B. Choi, Y.-R. Lee, Y.-T. Chang, C.-H. Kim, M.A. Bae, J.H. Ahn, Chem. Commun. 47 (2011) 7500–7502.

[19] F. Piscitelli, A. Ligresti, G. La Regina, A. Coluccia, L. Morera, M. Allarà, E. Novellino, V.D. Marzo, R. Silvestri, J. Med. Chem. 55 (2012) 5627–5631.

[20] A. Bruel, C. Logé, M.-L. de Tauzia, M. Ravache, R. Le Guevel, C. Guillouzo, J.-F. Lohier, J.S. de Oliveira Santos, O. Lozach, L. Meijer, S. Ruchaud, H. Bénédetti, J.-M. Robert, Eur. J. Med. Chem. 57 (2012) 225–233.

[21] Q. Tian, N.K. Nayyar, S. Babu, L. Chen, J. Tao, S. Lee, A. Tibbetts, T. Moran, J. Liou, M. Guo, T.P. Kennedy, Tetrahedron Lett. 42 (2001) 6807–6809.

[22] S.E. Webber, K. Okano, T.L. Little, S.H. Reich, Y. Xin, S.A. Fuhrman, D.A. Matthews, R.A. Love, T.F. Hendrickson, A.K. Patick, J.W. Meador III, R.A. Ferre, E.L. Brown, C.E. Ford, S.L. Binford, S.T. Worland, J. Med. Chem. 41 (1998) 2786–2805.

[23] U. Bacha, J. Barrila, B. Gabelli, Y. Kiso, L.M. Amzel, E. Freire, Chem. Biol. Drug Des. 72 (2008) 34–39.

[24] J. Barrila, U. Bacha, E. Freire, Biochemistry 45 (2006) 14908–14916.

[25] K. Akaji, H. Konno, M. Onozuka, A. Makino, H. Saito, K. Nosaka, Bioorg. Med. Chem. 16 (2008) 9400–9408.

[26] K. Akaji, H. Konno, H. Mitsui, K. Teruya, Y. Shimamoto, Y. Hattori, T. Ozaki, M. Kusunoki, A. Sanjoh, J. Med. Chem. 54 (2011) 7962–7973.

[27] H. Yang, W. Xie, X. Xue, K. Yang, J. Ma, W. Liang, Q. Zhao, Z. Zhou, D. Pei, J. Ziebuhr, R. Hilgenfeld, K.Y. Yuen, L. Wong, G. Gao, S. Chen, Z. Chen, D. Ma, M. Bartlam, Z. Rao, PLoS Biol. 3 (2005) 1742–1752.